BATF-dependent IL-7R^{hi}GM-CSF^{+} T cells control intestinal graft-versus-host disease

Evelyn Ullrich,[1,2,3] Benjamin Abendroth,[4] Johanna Rothamer,[1,2,3] Carina Huber,[4] Maike Büttner-Herold,[5] Vera Buchele,[4] Tina Vogler,[4] Thomas Longerich,[6] Sebastian Zundler,[4] Simon Völkl,[1] Andreas Beilhack,[7] Stefan Rose-John,[8] Stefan Wirtz,[4] Georg F. Weber,[9] Sakhila Ghimire,[10] Marina Kreutz,[10] Ernst Holler,[10] Andreas Mackensen,[1] Markus F. Neurath,[4] and Kai Hildner[4]

[1]Department of Medicine 5, University Hospital Erlangen, University of Erlangen-Nuremberg, Erlangen, Germany. [2]Children's Hospital, Department of Pediatric Stem Cell Transplantation and Immunology, and [3]LOEWE Center for Cell and Gene Therapy, Johann Wolfgang Goethe University, Frankfurt, Germany. [4]Department of Medicine 1, University Hospital Erlangen, University of Erlangen-Nuremberg, Kussmaul Campus for Medical Research, Erlangen, Germany. [5]Institute of Pathology, Department of Nephropathology, University Hospital Erlangen, Erlangen, Germany. [6]Institute of Pathology, University Hospital Heidelberg, Heidelberg, Germany. [7]Center for Interdisciplinary Clinical Research, Würzburg University, Würzburg, Germany. [8]Institute of Biochemistry, Christian-Albrechts-University, Kiel, Germany. [9]Department of Surgery, University Hospital Erlangen, University of Erlangen-Nuremberg, Erlangen, Germany. [10]Department of Hematology and Oncology, University Hospital Regensburg, Regensburg, Germany.

Acute graft-versus-host disease (GVHD) represents a severe, T cell–driven inflammatory complication following allogeneic hematopoietic cell transplantation (allo-HCT). GVHD often affects the intestine and is associated with a poor prognosis. Although frequently detectable, proinflammatory mechanisms exerted by intestinal tissue–infiltrating Th cell subsets remain to be fully elucidated. Here, we show that the Th17-defining transcription factor basic leucine zipper transcription factor ATF-like (BATF) was strongly regulated across human and mouse intestinal GVHD tissues. Studies in complete MHC-mismatched and minor histocompatibility–mismatched (miHA-mismatched) GVHD models revealed that BATF-expressing T cells were functionally indispensable for intestinal GVHD manifestation. Mechanistically, BATF controlled the formation of colon-infiltrating, IL-7 receptor–positive (IL-7R^{+}), granulocyte-macrophage colony-stimulating factor–positive (GM-CSF^{+}), donor T effector memory (Tem) cells. This T cell subset was sufficient to promote intestinal GVHD, while its occurrence was largely dependent on T cell–intrinsic BATF expression, required IL-7–IL-7R interaction, and was enhanced by GM-CSF. Thus, this study identifies BATF-dependent pathogenic GM-CSF^{+} effector T cells as critical promoters of intestinal inflammation in GVHD and hence putatively provides mechanistic insight into inflammatory processes previously assumed to be selectively Th17 driven.

Introduction

Allogeneic hematopoietic cell transplantation (allo-HCT) often represents the only therapeutic option to cure severe hematopoietic diseases. The overall outcome of allo-HCT is largely determined by the frequency of relapses of the malignant disorder and the severity of infection- or graft-versus-host disease–associated (GVHD-associated) complications (1–3). Especially severe forms of intestinal GVHD are associated with high mortality rates (4). Donor T cells have been shown to critically promote inflammation that induces fatal GVHD-associated tissue damage manifesting, for example, in the gut (intestinal GVHD) (1, 3). While these observations indicate that T cells represent a potential target to mitigate GVHD development and severity, detailed knowledge on the cues driving donor T cell differentiation into GVHD-mediating effector cell subsets is still limited.

We have previously identified the AP-1 transcription factor basic leucine zipper transcription factor ATF-like (BATF) to be a critical regulator of Th17 development and a promoter of colitis-associated carcinomas (5, 6). Among Th cell subsets, Th17 cells have been implicated in the mediation of tissue destruction in a wide range of inflammatory diseases including inflammatory bowel disease (IBD) (7–9). In support of the functional relevance of Th17 cell biology in intestinal inflammation, specific targeting of the Th17 differentiation–regulating transcription factor RORγt limited experimental colitis (7, 10). However, whether alloreactive Th17 cells promote GVHD-associated intestinal inflammation is a matter of controversy, since independent studies yielded partially contradictory results (7–9, 11–15).

In this study, we sought to functionally assess the T cell–intrinsic role of BATF in acute murine GVHD model systems. We found that BATF-expressing T cells are indispensable for intestinal GVHD development. However, to our surprise, our mechanistic studies revealed that BATF controlled the formation of a distinct IL-7 receptor (IL-7R) signaling–responsive GM-CSF^{+} T cell subset, thus opening up new avenues for therapeutic interventions to attenuate intestinal GVHD.

▶ Related Commentary: p. 897

Authorship note: E. Ullrich and B. Abendroth contributed equally to this work.
Conflict of interest: The authors have declared that no conflict of interest exists.
Submitted: June 23, 2016; **Accepted:** December 12, 2017.
Reference information: *J Clin Invest*. 2018;128(3):916–930.
https://doi.org/10.1172/JCI89242.

Results

BATF-expressing donor T cells control acute GVHD. Interestingly, gene expression–profiling experiments revealed enhanced *BATF* transcript levels within intestinal GVHD–affected compared with

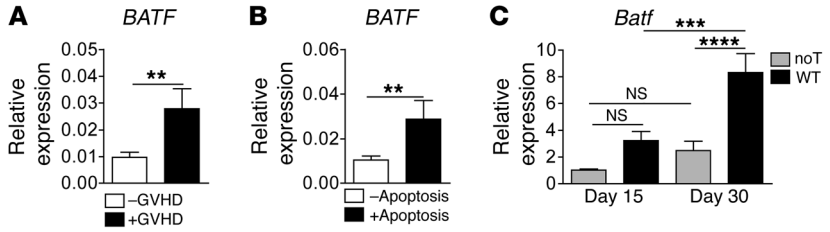

Figure 1. Intestinal GVHD is linked to *BATF/Batf* expression in humans and mice. (**A** and **B**) Quantitative gene expression analyses of human *BATF* transcripts in colonic tissue biopsies derived from allo-HCT patients. Samples were categorized by (**A**) the histopathologic absence (–GVHD, n = 30 samples) or presence (+GVHD, n = 22 samples) of GVHD-associated lesions and by (**B**) the absence (–Apoptosis, n = 32 samples) or presence (+Apoptosis, n = 20 samples) of GVHD severity–related epithelial cell apoptosis. Data represent the mean ± SEM of normalized relative *BATF* expression levels calculated from a standard curve. (**C**) Murine *Batf* gene expression kinetics in colonic tissue from GVHD-induced mice (days 15 and 30) after transplantation of 5×10^6 allogeneic T cell–depleted CD45.1 B6.SJL WT BM on day 1 into total body–irradiated (8 Gy) BALB/c mice the day before, followed by adoptive transfer of 0.7×10^6 C57Bl/6 alloreactive WT donor $CD3^+$ T cells (WT) or no T cells (noT) on day 2. Gene expression levels in colonic tissue represent the normalized relative fold-change in expression compared with day-15 colonic tissue expression in mice without donor T cell transfer (noT), with the expression level arbitrarily set at 1. Data represent the mean ± SEM and were derived from day-15 noT (n = 13) and WT (n = 14) and from day-30 noT (n = 15) and WT (n = 12) individual mice per group and are derived from at least 3 independent experiments. $^{**}P < 0.01$, $^{***}P < 0.001$, and $^{****}P < 0.0001$, by unpaired, 2-sided Student's t test (**A** and **B**) and 1-way ANOVA with Bonferroni's multiple comparisons post test (**C**).

–unaffected colonic tissues from allo-HCT patients. Upregulated *BATF* expression was associated with an increased prevalence of apoptotic cells, indicating a more severe intestinal GVHD course (Figure 1, A and B). Similarly, we detected increased colonic *Batf* colonic tissue expression levels over the course of acute, GVHD-induced colitis in a mouse model of complete MHC–mismatched bone marrow transplantation (allo-BMT) plus allogeneic T cell transfer (Figure 1C and Supplemental Figure 1; supplemental material available online with this article; https://doi.org/10.1172/JCI89242DS1). Overall, these observations imply an across-species conserved regulation of BATF expression during acute GVHD–associated colitis.

To test the functional relevance of this finding, we compared GVHD development following transplantation of allogeneic WT and $Batf^{-/-}$ donor $CD3^+$ T cells in a complete MHC–mismatched setting. Importantly, up to 67 days after allo-HCT, $Batf^{-/-}$ T cells elicited only mild clinical GVHD and allowed normal immune reconstitution and long-term survival compared with that observed in WT T cell–recipient mice (Figure 2, A and B, and Supplemental Figure 2A). Donor T cell–restricted BATF deficiency significantly diminished endoscopic signs of colitis at the onset (day 15) and macroscopic (colon length), endoscopic, and histologic signs of intestinal inflammation at full clinical manifestation (day 30) of GVHD (Figure 2, A–E, and Supplemental Figure 2, A–C), indicating overall that BATF-dependent T cells are critical mediators of GVHD-mediated tissue damage affecting predominately lymphoid organs and the intestines. Interestingly, *Il6*, but not *Tnfa* or *Il17a*, colon tissue expression levels were hampered in the absence of BATF-expressing T cells (Figure 3A). Similarly, $Batf^{-/-}$ T cells failed to upregulate systemic IL-6 serum levels, while TNF-α and IL-17A levels were largely indistinguishable between WT and $Batf^{-/-}$ donor T cell–receiving mice (Figure 3B).

Consecutively, we assessed the role of BATF in a minor histocompatibility–mismatched (miHA-mismatched) GVHD model system. To this end, we transplanted WT or $Batf^{-/-}$ allogeneic T cells into irradiated BALB.b ($H\text{-}2^b$) mice (16). Importantly, BATF deficiency attenuated both the clinical score and signs of intestinal GVHD (Figure 4, A and B, and Supplemental Figure 3A), while GVHD-associated liver histopathology was indistinguishable between WT and $Batf^{-/-}$ T cell–treated mice (Figure 4C and Supplemental Figure 3B). Together, donor T cell–intrinsic BATF critically promotes intestinal GVHD in both complete MHC– and miHA-mismatched model systems.

BATF drives the formation of a GVHD-promoting T cell pool distinct from Th17 cells. To shed light on the underlying mechanisms, we first excluded the possibility that $Batf^{-/-}$ $CD3^+$ donor T cells either contained greater numbers of memory cells prior to transfer or preferentially differentiated into $FoxP3^+$ Tregs after transfer (Supplemental Figure 4, A and B) (17, 18). Second, we explored the possibility that altered in vivo expansion, intestinal homing, or tissue migration accounted for attenuated GVHD formation in the absence of BATF (9, 16, 19). Using both bioluminescence imaging and flow cytometry, we observed comparable in situ T cell expansion and gut-homing receptor expression profiles in both the mesenteric lymph node (MLN) and colonic lamina propria (cLP) within the first 2 weeks after allo-HCT, resulting in a BATF-independent pool of proliferating Ki-67^+ cLP T cells (Figure 5, A–E, and Supplemental Figure 5, A and B). Intravital confocal microscopy studies revealed that cotransferred WT and $Batf^{-/-}$ donor T cells homed and transmigrated to the colonic tissue in an indistinguishable manner (Figure 5F). Together, these results largely exclude defective proliferation, gut imprinting (19), and transmigratory behavior as key mechanisms underlying abrogated intestinal GVHD in the absence of BATF. However, upon clinical disease onset on day 15, we observed that further donor T cell expansion was hampered in mice receiving BATF-deficient T cells (Figure 5, A, B, and E), implying that this failure might be secondary to the inability of T cells to mediate intestinal GVHD. To evaluate this option, we characterized the T cell response in more detail. Sort-purified $CD4^+$ cLP–resident donor T cells on day 15, i.e., around GVHD onset, expressed expectedly low *Il17a* levels in the absence of BATF, while IFN-γ and TNF-α gene and protein expression, respectively, in both MLN- and cLP-resident T cells was regulated in a BATF-independent manner (Figure 6, A–C). In striking contrast, BATF deficiency abrogated donor T cell–intrinsic IL-6 and GM-CSF transcript and protein expression levels during early-phase (day 15) and late-phase (day 30) GVHD (Figure 6, A–E). Interestingly, $CD4^+$ T cells represented the primary source of T cell–derived GM-CSF (Figure 6F). And importantly, BATF-dependent regulation of GM-CSF expression was due to a cell-intrinsic mechanism (Figure 6G) and encompassed multiple IFN-γ– and TNF-α–coexpressing subsets, while $GM\text{-}CSF^-$ T cell subsets remained largely unaffected

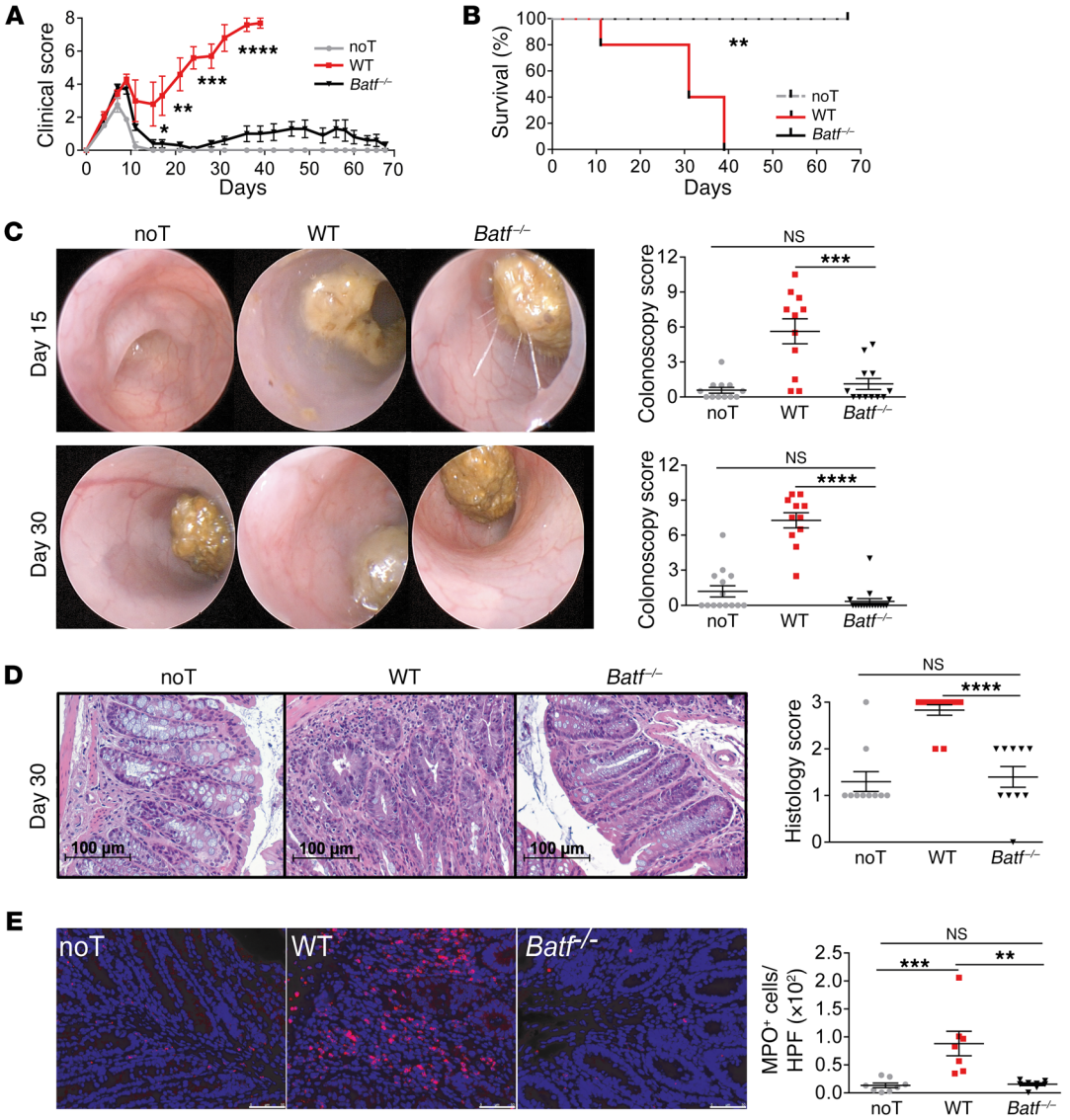

Figure 2. Acute GVHD is critically dependent on BATF-expressing donor T cells. (**A** and **B**) Clinical GVHD score (**A**) and survival (**B**) following transfer of allogeneic WT (red squares) and *Batf*$^{-/-}$ (black triangles) CD3^{+} C57Bl/6 donor T cells or no T cells (gray circles) into irradiated BALB/c mice after transplantation of T cell–depleted CD45.1 B6.SJL WT BM. Results from 1 representative experiment (n = 5 mice/group) of at least 4 independent experiments are shown. (**C** and **D**) Endoscopic (**C**) and histologic (**D**) assessment of GVHD-associated colitis activity at the onset of GVHD on day 15 (**C**, upper row) and when GVHD was fully established on day 30 (**C**, lower row). Representative images are shown, and scatter plots summarize the pooled results of colonoscopy scores derived from 3 independent experiments for day 15 (n = 12 noT mice; n = 11 WT mice; n = 12 *Batf*$^{-/-}$ mice) and from 2 independent experiments for day 30 (n = 14 noT mice; n = 11 WT mice; n = 17 *Batf*$^{-/-}$ mice). (**D**) In analogy, representative histopathologic cross-sections of the colon of each individual group 30 days after GVHD induction (C57Bl/6 in BALB/c) are shown, while scatter plots show the pooled histology scores from 3 independent experiments with noT (n = 10), WT (n = 12), and *Batf*$^{-/-}$ (n = 10) mice. Scale bars: 100 μm. (**E**) Detection and quantification of MPO^{+} cells in colonic tissue sections from the GVHD-prone BALB/c mice described in **A**. Scale bars: 50 μm. Scatter plots show the mean ± SEM of MPO^{+} cells/HPF representing pooled data for 7 to 8 mice per group from 3 independent experiments. Data represent the mean ± SEM. *P < 0.05, **P < 0.01, ***P < 0.001, and ****P < 0.0001, by 2-sided, unpaired Student's t test (**A**) and 1-way ANOVA with Bonferroni's multiple comparisons post test (**B**–**E**).

in the absence of BATF (Supplemental Figure 6). Strikingly, in the miHA-mismatched GVHD model, GM-CSF^{+}, but not IFN-γ^{+}, T cell subsets were equally dependent on BATF (Supplemental Figure 7, A and B). Collectively, BATF drives the generation of a unique intestinal donor T cell population distinct from Th17 cells and characterized by GM-CSF expression.

T cell–derived GM-CSF promotes acute GVHD. To assess whether reduced GM-CSF might account for hampered GVHD formation in the absence of T cell–intrinsic BATF expression, *Batf*$^{-/-}$ T cell–recipient mice were repetitively treated with either recombinant GM-CSF or vehicle alone. Strikingly, GM-CSF complementation partially reconstituted both systemic and intestinal signs of GVHD in *Batf*$^{-/-}$ T cell–treated mice (Figure 7, A and B).

To directly assess the contribution of T cell–derived GM-CSF, we compared GVHD development upon transfer of WT or *Csf2*$^{-/-}$ donor T cells. Importantly, *Csf2*$^{-/-}$ T cell–recipient mice showed attenuated systemic GVHD and significantly increased survival rates compared with WT controls (Figure 7, C and D). Further-

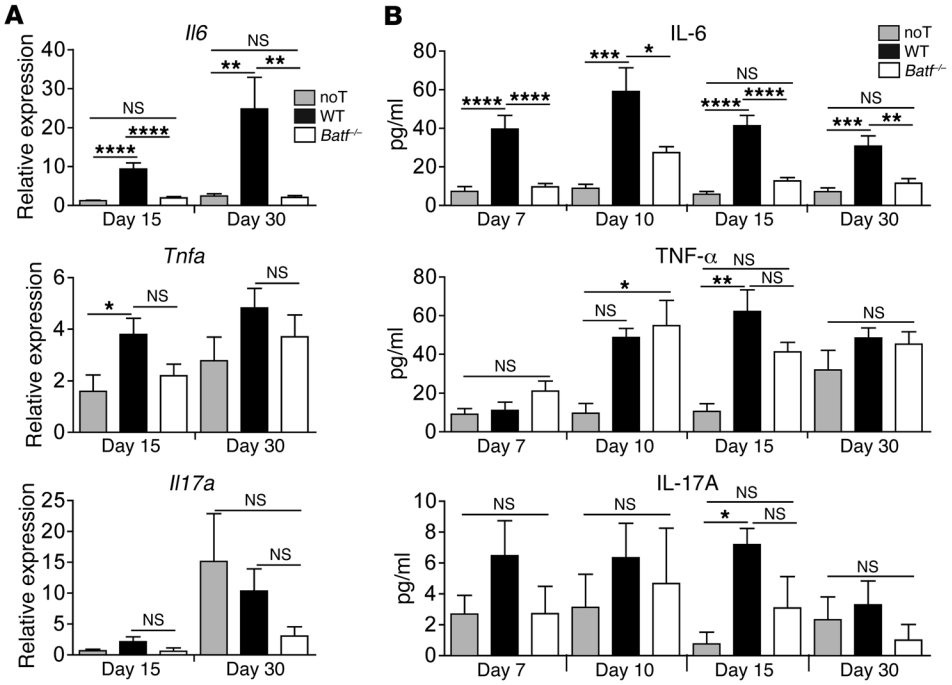

Figure 3. BATF deficiency–related GVHD attenuation leads to reduced systemic and intestinal IL-6 expression. (**A**) *Il6*, *Tnfa*, and *Il17a* transcript levels in colonic tissues were determined by qPCR upon GVHD onset (day 15) and during (day 30) established GVHD–associated colitis following transfer of allogeneic WT (black bars) and *Batf*$^{-/-}$ (white bars) CD3$^+$ C57Bl/6 donor T cells or no T cells (light gray bars). Gene expression levels were normalized to the expression levels that were detected on day 15 in the noT mice, with an arbitrarily determined expression level of 1. Error bars represent the mean ± SEM of pooled data from at least 3 independent experiments. Results represent *Il6* expression (n = 13 noT, n = 12 WT, and n = 11 *Batf*$^{-/-}$ mice/time point); *Tnfa* expression (n = 8 noT, n = 10 WT, and n = 11 *Batf*$^{-/-}$ mice/time point); and *Il17a* expression (n = 4 noT, n = 10 WT, and n = 11 *Batf*$^{-/-}$ mice/time point). (**B**) IL-6, TNF-α, and IL-17A serum cytokine levels in the mice described in **A** were assessed by flow cytometry on days 7, 10, 15, and 30. Error bars represent the mean ± SEM. Results represent pooled data from 3 independent experiments for IL-6 measurements (n = 7 noT, n = 8 WT, and n = 12 *Batf*$^{-/-}$ individual mice/time point); TNF-α measurements (n = 3 noT, n = 4 WT, and n = 4 *Batf*$^{-/-}$ individual mice/time point); and IL-17A measurements (n = 6 noT, n = 6 WT, and n = 6 *Batf*$^{-/-}$ individual mice/time point). *P < 0.05, **P < 0.01, ***P < 0.001, and ****P < 0.0001, by 1-way ANOVA with Bonferroni's and Dunn's multiple comparisons post tests.

more, endoscopic signs of intestinal GVHD were reduced, particularly during established GVHD (Figure 7E). Interestingly, both *Il6* tissue expression levels and the intestinal IL-6$^+$ donor T cell pool were indistinguishable between both groups (Figure 7, F and G). Together, our data demonstrate that T cell–derived GM-CSF promotes acute GVHD, thereby affecting survival as well as systemic and intestinal manifestations.

BATF controls the formation of an IL-7R^{hi} GM-CSF$^+$ T cell pool. Having shown that BATF identified to control the GM-CSF$^+$ donor T cell pool in vivo, we studied whether IL-7–driven GM-CSF$^+$ T cell formation was affected in the absence of BATF (20). While IL-7R/*Il7r* expression kinetics was unaltered in vitro, the pool of IL-7–induced GM-CSF$^+$ T cells was diminished in the absence of BATF after 5 days of culture (Figure 8A, and Supplemental Figure 8, A and B). Consistent with this in vitro kinetics, we found that, already by day 7, i.e., 5 days after T cell transfer, the in vivo pool of intestinal GM-CSF$^+$ donor T cells was reduced in the absence of T cell–intrinsic BATF expression in GVHD-prone mice (Figure 8B). However, further studies revealed that both the median fluorescence intensity of the IL-7R expressed by GM-CSF$^+$ donor T cells and specifically the relative and absolute pool of MLN- and cLP-residing IL-7R^{hi}GM-CSF$^+$ donor T cells were significantly diminished in the absence of BATF upon both disease onset (day 15) and during established intestinal GVHD (Figure 8, C and D, and Supplemental Figure 8C). In contrast, both IL-7R$^{-/lo}$GM-CSF$^+$ and IL-7R^{hi}GM-CSF$^-$ donor T cell fractions were virtually unaffected by BATF deficiency (Supplemental Figure 8, D and E).

Consistent with an activated and proinflammatory state, the majority of IL-7R^{hi}GM-CSF$^+$ T cells coexpressed IFN-γ and TNF-α or expressed either cytokine alone in a largely BATF-independent manner (Supplemental Figure 9, A and B). Interestingly, donor-derived intestinal T cells predominately had a CD44$^+$CD62L$^-$ phenotype, i.e., they were enriched for T effector and T effector memory (Tem) cells in a BATF-dependent manner (Figure 8E). Together, in the absence of BATF, the donor colonic T cell pool within GVHD-prone mice largely lacks IL-7R^{hi}GM-CSF$^+$ T cells and is deprived of Tem cells.

IL-7–IL-7R interaction regulates intestinal GVHD–promoting GM-CSF$^+$ Tem cells. Given the IL-7R^{hi} expression status of intestinal donor T cells, we reasoned that IL-7–IL-7R interaction is required for the expansion and/or maintenance of GVHD-promoting GM-CSF$^+$ donor T cells, putatively providing a mechanistic explanation for the incomplete GVHD protection in the absence of *Csf2*$^{-/-}$ compared with *Batf*$^{-/-}$ T cells. To directly address this hypothesis, we treated GVHD-prone mice with an anti–IL-7R antibody until day 15, i.e., around clinical GVHD onset, alone or in combination with a GM-CSF–blocking antibody that was given over the entire course of the experiment. GVHD formation was compared with isotype IgG–treated mice and with untreated mice given *Batf*$^{-/-}$ donor T cells alone (Supplemental Figure 10A). Importantly, IL-7R blockade alone transiently attenuated GVHD (Figure 9A). However, treatment discontinuation resulted in a relapse of systemic and intestinal GVHD (Figure 9, A–C). In contrast, combined antibody-mediated IL-7R and GM-CSF blockade strongly and persistently suppressed systemic and intestinal GVHD and resulted in overall improved survival, indicating a beneficial, putative sequential cooperativity of both interventional strategies (Figure 9, A–D). Consistent with a relevant role of IL-7R signaling in the formation of GM-CSF$^+$ T cells, the frequency of GM-CSF$^+$ T cells within the cLP T cell compartment was significantly reduced by IL-7R blockade alone (Figure

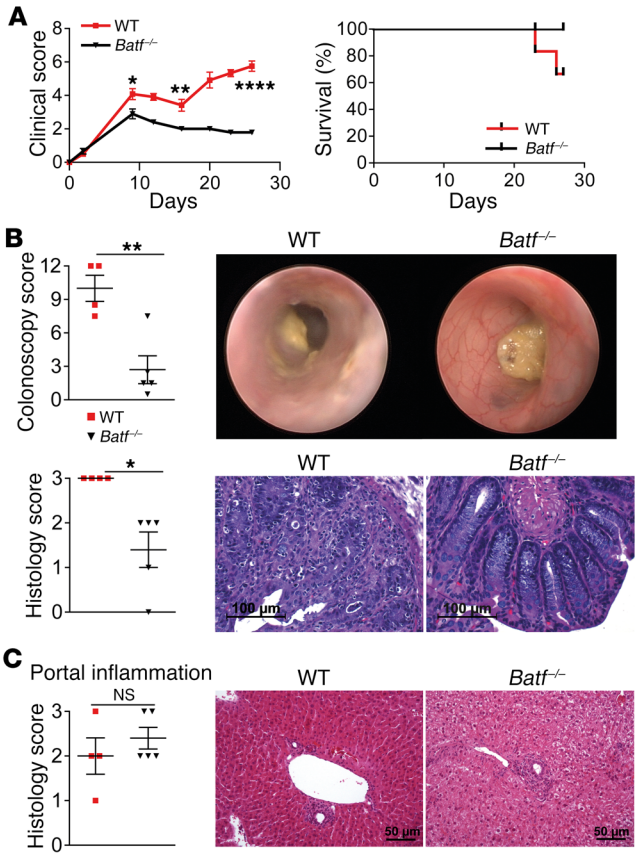

Figure 4. BATF-expressing T cells control intestinal but not hepatic GVHD in a miHA-mismatched model. (**A**) Clinical GVHD score and survival rates following transfer of allogeneic WT (red squares) and *Batf* $^{-/-}$ (black triangles) CD3$^+$ C57Bl/6 donor T cells into irradiated H-2b$^+$ BALB.b mice after transplantation of T cell–depleted CD45.1$^+$ B6.SJL WT BM. Results from 1 representative experiment are shown (n = 6 WT and n = 5 *Batf*$^{-/-}$ mice). (**B**) Representative endoscopic (upper row) and histologic cross-sectional (lower row) images showing GVHD-associated colitis activity during established GVHD on day 27. Scatter plots summarize the pooled results of colonoscopy and histology scores for WT (n = 4) and *Batf*$^{-/-}$ (n = 5) T cell–recipient mice. Scale bars: 100 μm. (**C**) Histopathologic evaluation of GVHD-associated liver lesions (scatter plot) assesses portal inflammation of the liver, and representative images of histopathologic cross-sections are shown. Scale bars: 50 μm. Data represent the mean ± SEM. $^*P < 0.05$, $^{**}P < 0.01$, and $^{****}P < 0.0001$, by 2-sided, unpaired Student's t test.

9E). However, in contrast to the combined blockade of IL-7R and GM-CSF, IL-7R blockade alone failed to diminish both the absolute size of the GM-CSF$^+$ LP T cell pool in GVHD-affected mice (Figure 9F) and the total intestinal donor T cell numbers both upon and after GVHD onset (Supplemental Figure 10B and Figure 9G). Finally, given the reduced Tem cell pool in the absence of BATF and the established role of IL-7 during the transition of regular effector cells to Tem cells (21–23) previously shown to potently promote GVHD (24), we wondered whether single or combined antibody-mediated IL-7R blockade restrained the donor-derived Tem cell pool. Interestingly, we found that the intestinal donor Tem cell pool was virtually indistinguishable between isotype control–treated mice and mice treated with the anti–IL-7R antibody alone (Figure 9H). This result largely excludes the possibility that anti–IL-7R treatment alone leads to an unselective and/or global depletion of Tem cells in the gut. However, combined inhibition of IL-7R and GM-CSF markedly reduced absolute Tem cell numbers, suggesting that a putatively indirect, though at least in part GM-CSF–driven, mechanism regulates the donor Tem cell pool in vivo. Collectively, these data suggest that, in addition to its role described in vitro, IL-7R signaling is involved in the regulation of GM-CSF$^+$ T cell formation in vivo. However, the magnitude and GVHD-mediating potential of the GM-CSF$^+$ T cell pool are further regulated by additional signals including GM-CSF itself.

IL-7R^{hi}GM-CSF$^+$ cLP T cells are sufficient to elicit intestinal GVHD. To directly demonstrate that T cells are the most relevant GM-CSF–producing source responsible for intestinal GVHD manifestation, we treated WT and *Csf2*$^{-/-}$ donor T cell–recipient mice with IL-7R–blocking antibodies. Strikingly, T cell–restricted GM-CSF deficiency alone significantly reduced systemic and intestinal GVHD by both endoscopic and histologic measurements (Figure 10, A–C, and Supplemental Figure 11A). In addition, the total numbers of donor-derived cLP T cells were significantly lower in *Csf2*$^{-/-}$ mice than in WT donor T cell–recipient mice (Figure 10D). Furthermore, the pool of *Csf2*$^{-/-}$ T cells expressing IFN-γ and TNF-α, respectively, was diminished compared with the WT T cell pool (Figure 10E and Supplemental Figure 11B). In summary, these data fully reproduced and extended our results obtained with systemic antibody–mediated GM-CSF blockade, suggesting that IL-7–responsive GM-CSF2$^+$ donor T cells directly mediate intestinal GVHD. Therefore, we reasoned that IL-7R^{hi} GM-CSF2$^+$ donor T cells might be sufficient to restore intestinal GVHD in *Batf*$^{-/-}$ donor T cell–treated mice. To directly test this hypothesis, we sort purified CD45.1$^+$IL-7R^{hi} cLP T cells from mice with severe intestinal GVHD and transferred those T cells into mice that had received CD45.2$^+$ *Batf*$^{-/-}$ donor T cells lacking GVHD-inducing abilities 10 days earlier. Strikingly, IL-7R^{hi} T cells largely reestablished systemic and intestinal GVHD when compared with vehicle-treated control mice (Figure 10, F–H). Interestingly, the presence of GVHD-reconstituting WT T cells did not rescue GM-CSF expression within *Batf*$^{-/-}$ T cells, again indicating that hampered GM-CSF expression is due to a T cell–intrinsic, BATF-dependent mechanism. However, IL-7R^{hi} cLP WT T cells significantly increased the absolute pool of GM-CSF–expressing T cells (Figure 10I). Together, these results show that IL-7R^{hi}GM-CSF–expressing cLP T cells are sufficient to mediate intestinal GVHD and are able to reestablish colitis in *Batf*$^{-/-}$ donor T cell–recipient mice.

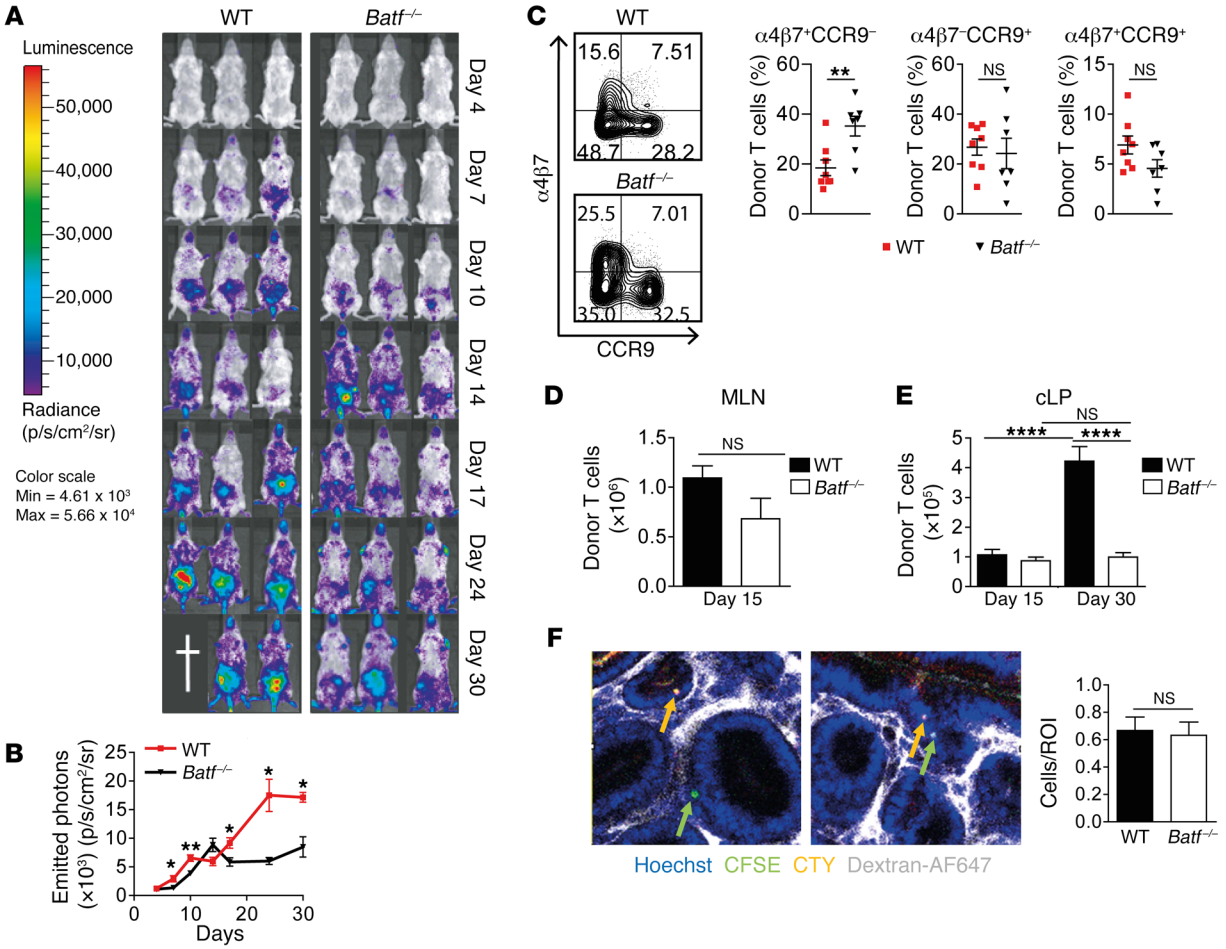

Figure 5. BATF is dispensable for early, but not late, donor T cell expansion. (**A** and **B**) Donor T cell expansion was assessed by in vivo BLI in GVHD-prone mice (C57Bl/6 in BALB/c) after adoptive transfer of luciferase-expressing WT and *Batf*$^{-/-}$ CD3$^+$ T cells. (**A**) Representative images show 3 mice of 6 independently analyzed mice/group. (**B**) Mean values ± SEM of emitted photons detected (n = 6 mice/group). (**C**) WT (red squares) and *Batf*$^{-/-}$ (black triangles) CD3$^+$C57Bl/6 T cells were transferred into CD45.1$^+$ allo-BMT BALB/c mice. On day 12, α4β7$^+$ and CCR9$^+$ expression of MLN-resident H-2d$^-$CD45.1$^-$CD3$^+$CD4$^+$ donor T cells was assessed by flow cytometry. Scatter plots represent the mean ± SEM of the indicated subsets derived from 2 experiments (n = 8 WT and n = 7 *Batf*$^{-/-}$ mice). (**D** and **E**) Absolute CD45.2$^+$CD3$^+$CD4$^+$ donor T cell numbers (C57Bl/6 in BALB/c) within MLN (day 15) and cLP (day 15 and day 30) were calculated by flow cytometry. Error bars represent the mean ± SEM of pooled data. (**D**) n = 6 mice/genotype and (**E**) n = 19 WT mice and n = 20 *Batf*$^{-/-}$ mice (day 15); n = 28 WT mice and n = 21 *Batf*$^{-/-}$ mice (day 30). (**F**) Allo-HCT (*Rag1*$^{-/-}$ BM) BALB/c mice received a 1:1 mixture of CFSE$^+$ WT and CTY$^+$ *Batf*$^{-/-}$ CD4$^+$ T cells. One hour later, donor T cell tissue homing and migration were assessed by in vivo confocal microscopy (2 representative images are shown; Hoechst-stained nuclei are shown in blue, dextran-AF647–stained vasculature in white, CFSE-stained WT T cells in green, and CTY-stained *Batf*$^{-/-}$ T cells in orange, with the latter 2 indicated by colored arrows). Bar graph indicates donor T cell frequencies (n = 5 ROI/mouse; n = 6 mice/genotype). *P < 0.05, **P < 0.01, and ****P < 0.0001, by 2-sided, unpaired Student's t test (**B**–**D** and **F**) and 1-way ANOVA with Bonferroni's multiple comparisons post test (**E**).

Collectively, the results presented in this study demonstrate that BATF drives intestinal, IL-7 signaling–responsive and GM-CSF–producing donor T cell formation, with an effector memory phenotype that promotes acute intestinal GVHD.

Discussion

T cells phenotypically defined as Th17 cells are widely distributed within inflamed tissues throughout the body (25). The identification of Th17 cells and the discovery that Th17 cell–directed therapeutic strategies are highly effective to attenuate tissue inflammation have revolutionized the concepts of the pathogenesis of immune-mediated diseases (26). The transcription factor BATF was shown to control Th17 cell differentiation and regulate inflammation-associated colon tumor formation (5, 6). In the context of alloreactivity-mediated tissue damage, Th17 cells have been implicated in playing a disease-promoting role, although this interpretation is not undisputed (11–15). The contribution of BATF-dependent T cell responses in this setting has not been addressed.

First, we performed gene expression analyses and found that BATF expression is strongly induced within GVHD-affected colonic tissues derived from mice and humans undergoing allo-HCT. Given that BATF is predominately expressed by lymphoid lineages (6), we hypothesized that BATF-expressing T cells might contribute to this enhanced expression, prompting us to study the functional relevance of donor T cell–intrinsic BATF in GVHD manifestation. Here, using both complete MHC– and miHA-mismatched GVHD models, we demonstrate that BATF is indispensable for the manifestation of intestinal GVHD. While homing of *Batf*$^{-/-}$ T cells to the small intes-

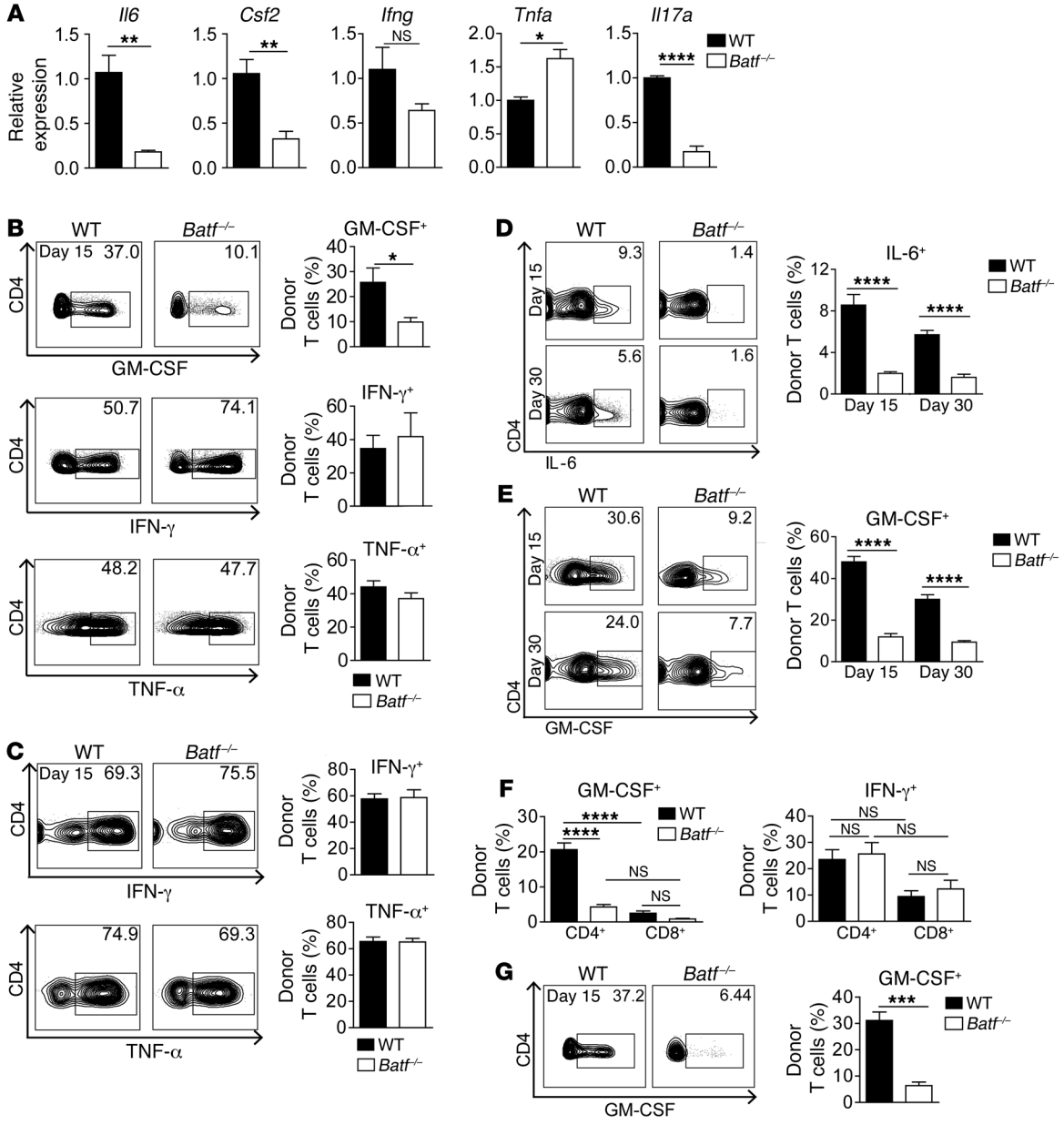

Figure 6. Donor T cells express IL-6 and GM-CSF in a BATF-dependent manner. (**A**) *Il6*, *Csf2*, *Ifng*, *Tnfa*, and *Il17a* gene expression in FACS-purified, donor-derived LP WT (black) and *Batf*$^{-/-}$ (white) CD4$^+$ T cells from GVHD-prone mice (C57Bl/6 into BALB/c) were quantified on day 15. Expression represents normalized, relative fold-change expression compared with WT T cells (set at 1). Error bars represent the mean ± SEM of 3 samples per group from 2 independent experiments, with 6 mice per genotype. (**B**–**E**) Assessment of the pool of (**B**) GM-CSF–, IFN-γ–, and TNF-α–expressing H2d$^-$CD45.2$^+$CD4$^+$ donor MLN T cells (day 15); (**C**) IFN-γ– and TNF-α–expressing, donor-derived CD45.2$^+$CD3$^+$CD4$^+$ cLP T cells (day 15); and (**D**) IL-6– and (**E**) GM-CSF–expressing CD45.2$^+$CD3$^+$CD4$^+$ cLP T cells (days 15 and 30) from the GVHD-prone mice described in **A**. Bar graphs show the mean ± SEM of 6 mice per genotype (**B**); (**C**) IFN-γ (n = 10 WT and n = 11 *Batf*$^{-/-}$ mice) and TNF-α (n = 8 WT and n = 11 *Batf*$^{-/-}$ mice); (**D**) day 15 (n = 8 WT and n = 10 *Batf*$^{-/-}$ mice) and day 30 (n = 8 WT and n = 8 *Batf*$^{-/-}$ mice); (**E**) day 15 (n = 16 WT and n = 17 *Batf*$^{-/-}$ mice) and day 30 (n = 21 WT and n = 22 *Batf*$^{-/-}$ mice) from 3 independent experiments (**C**–**E**). (**F**) GM-CSF$^+$ and IFN-γ$^+$ H2d$^-$CD45.2$^+$CD4$^+$ and CD8$^+$ cLP donor T cells, respectively, from GVHD-prone mice were assessed by flow cytometry (day 15). Bar graphs show the mean ± SEM of 6 mice per genotype. (**G**) *Rag1*$^{-/-}$ BMT BALB/c mice received CD45.1$^+$ WT and CD45.2$^+$ *Batf*$^{-/-}$ donor C57Bl/6 T cells in a 1:1 mixture (day 2), and GM-CSF$^+$ H2d$^-$CD45.1$^+$ WT and CD45.2$^+$ *Batf*$^{-/-}$ CD4$^+$ T cell frequencies were determined (day 15). Representative contour plots and bar graph show the mean ± SEM (n = 7 mice). *P < 0.05, **P < 0.01, ***P < 0.001, and ****P < 0.0001, by 2-sided, unpaired Student's t test (**A**–**E**) and 1-way ANOVA with Bonferroni's multiple comparisons post test (**F**).

tine was described to be hampered under syngeneic conditions (9), we found the initial expansion and homing of alloreactive T cells to the cLP compartment to be largely unaffected in the absence of BATF. However, upon GVHD onset, the size of the donor colonic T cell population became increasingly BATF dependent. Hence, we reasoned that attenuated T cell proliferation might be secondary to the hampered T cell–intrinsic potential to induce and promote colitis. Interestingly, in addition to Th17 differentiation, we found that T cell–intrinsic GM-CSF and IL-6 expression of donor colonic T cells was highly dependent on BATF, while Th1 differentiation was

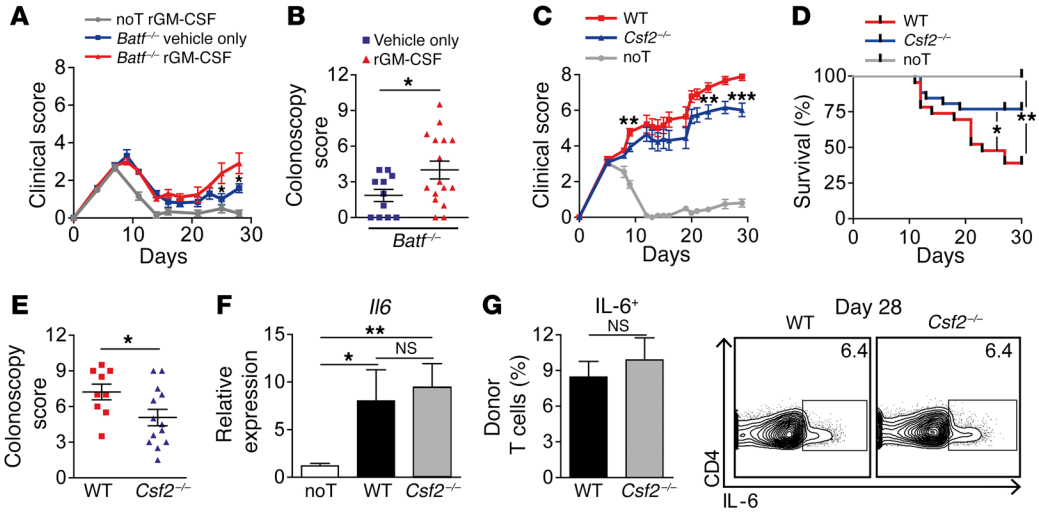

Figure 7. GM-CSF aggravates intestinal GVHD. (**A** and **B**) Assessment of systemic (clinical score, **A**) and intestinal (endoscopic score, **B**) GVHD of allo-BMT BALB/c mice that received *Batf*$^{-/-}$ donor CD3$^+$ T cells (red line and triangles) on day 2 (C57Bl/6 in BALB/c). *Batf*$^{-/-}$ T cell–treated mice received either daily i.p. injections (150 ng/injection) of recombinant GM-CSF (rGM-CSF) or vehicle only (red triangles and blue squares, respectively). As controls, noT mice (BMT only) received GM-CSF (gray line). Data from 2 independent experiments (n = 6 noT + rGM-CSF, n = 16 *Batf*$^{-/-}$ + rGM-CSF, and n = 11 *Batf*$^{-/-}$ + vehicle-only mice) are shown. (**C**–**E**) Systemic GVHD (clinical score, **C**), survival rates (**D**), and intestinal GVHD (endoscopic score, **E**) were assessed on day 28 in allo-BMT BALB/c mice treated with C57Bl/6 WT (red line and squares), *Csf2*$^{-/-}$ (blue line and triangles), or no (noT, gray line) CD3$^+$ donor T cells. Data from 2 independent experiments were pooled (n = 10 noT, n = 9 WT, and n = 13 *Csf2*$^{-/-}$ mice). (**F**) *Il6* gene expression levels were determined by qPCR analysis of colonic tissues 28 days after GVHD induction (C57Bl/6 in BALB/c), as described in **C**. Gene expression levels represent the normalized, relative fold-change of expression detected in noT mice (the expression level was arbitrarily set at 1). Bar graphs represent pooled data from 2 independent experiments (n = 9 noT; n = 8 WT, and n = 12 *Csf2*$^{-/-}$ mice. (**G**) IL-6–expressing, donor-derived CD45.2$^+$CD3$^+$CD4$^+$ LP T cell frequencies were determined by flow cytometry 28 days after GVHD induction, as described in **F**. Bar graphs indicate the mean ± SEM and represent pooled data from 2 independent experiments (n = 8 WT and n = 4 *Csf2*$^{-/-}$ mice). Representative contour plots show intracellular IL-6 levels in CD45.2$^+$CD3$^+$CD4$^+$ cLP T cells. *P < 0.05, **P < 0.01, and ***P < 0.001, by 2-sided, unpaired Student's t test (**A**–**E** and **G**) and 1-way ANOVA test with Dunn's multiple comparisons post test (**F**).

unaffected, as previously described (6). Functional studies involving cytokine reconstitution experiments with *Batf*$^{-/-}$ donor T cell–recipient mice and cytokine inactivation studies using *Csf2*$^{-/-}$ donor T cells clearly supported the idea that GM-CSF promotes the manifestation of GVHD-associated colitis. GM-CSF has been implicated as a critical T cell–derived effector cytokine that drives immune-mediated diseases such as multiple sclerosis (27, 28). Mechanistically, because of the absence of GM-CSF receptor expression by T cells themselves, it was suggested that the pathogenicity of T cell–derived GM-CSF is largely mediated through the recruitment and activation of inflammatory antigen-presenting cells via the upregulation of IL-1β, IL-6, and IL-23 expression, thereby further invigorating the expansion and maintenance of GM-CSF$^+$ T cells in a positive feedback loop (27–29). Consistent with a T cell–extrinsic, but GM-CSF–dependent, aggravation of GVHD, we found that the absence of T cell–intrinsic BATF expression and hence diminished GM-CSF$^+$ T cell numbers led to a reduced recruitment of myeloperoxidase-positive (MPO$^+$) myeloid cells to the gut.

Despite the GVHD-aggravating effects exerted by GM-CSF alone, GVHD attenuation induced by BATF-deficient donor T cells exceeded the reduced GVHD severity observed in the absence of T cell–intrinsic GM-CSF expression. One explanation for this discrepancy might be our finding that *Csf2*$^{-/-}$, in contrast to *Batf*$^{-/-}$, T cells are still able to express IL-6. In addition, IL-6 tissue expression levels in GVHD-affected colon were affected by T cell–restricted BATF, but not GM-CSF deficiency. Future studies need to further explore the functionality of IL-6 in these T cells.

While pathogenic Th17 cells were shown to be driven by IL-23 (30), GM-CSF$^+$ T cell–promoting signals are less well defined. Recently, IL-7 was described to control the formation of murine GM-CSF$^+$ T cells in a STAT5-dependent manner (20, 31). Importantly, we found that the IL-7–driven GM-CSF$^+$ T cell pool in vitro was diminished in the absence of BATF. In line with a functional role of IL-7–IL-7R interactions in regulating the GM-CSF$^+$ T cell pool also in vivo, we observed that anti–IL-7R–mediated blockade persistently reduced the fraction of GM-CSF$^+$ T cells within the donor T cell compartment. However, this treatment only transiently attenuated GVHD and failed to permanently restrain the absolute size of the GM-CSF$^+$ donor T cell pool. More pronounced GVHD-reducing effects resulting from IL-7/IL-7R blockade in vivo were reported by others and might be due to the continuous treatment regimen used in contrast to the transient anti–IL-7R antibody treatment method applied in our experimental setting (32). However, even continuous blockade of the IL-7–IL-7R interaction led to improved thymus-dependent immune reconstitution when compared with the control antibody–treated group (32). In line with this result, transient IL-7R blockade did not globally perturb intestinal T cell homeostasis. However, GVHD was sufficiently suppressed by a combined IL-7R and GM-CSF blockade, thus suggesting that a synergistic mechanism inhibits the formation, expansion, and functionality of intestinal GM-CSF$^+$ donor T cells. Importantly, studies using *Csf2*$^{-/-}$ T cells confirmed that T cells themselves are the most important source of GM-CSF, as the reduction in intestinal GVHD mirrored the results obtained

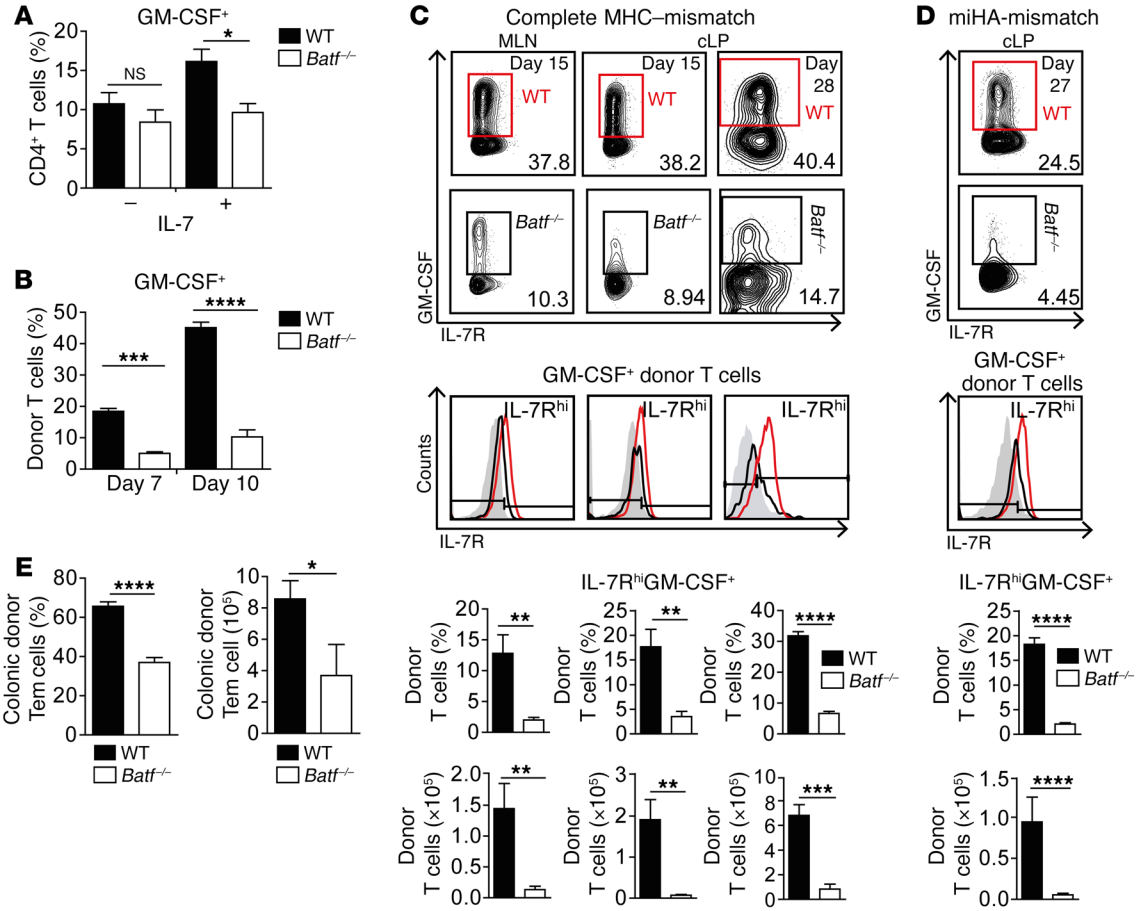

Figure 8. BATF controls the formation of IL-7R^{hi}GM-CSF$^+$ T cells. (**A**) GM-CSF$^+$CD4$^+$ T cell frequencies by intracellular flow cytometry on day 5 of in vitro culture under IFN-γ–neutralizing conditions, with or without IL-7. Bar graph represents pooled data from 4 independent experiments and indicates the mean ± SEM. Without IL-7 (–), n = 10 WT and n = 7 *Batf*$^{-/-}$ mice; with IL-7 (+), n = 16 WT and n = 12 *Batf*$^{-/-}$ mice. (**B**) GM-CSF–expressing, donor-derived CD45.2$^+$ CD3$^+$CD4$^+$ cLP T cell frequencies ex vivo in GVHD-prone mice after WT and *Batf*$^{-/-}$ CD3$^+$ donor T cell transfer (C57Bl/6 into BALB/c). Bar graph indicates the mean ± SEM of 4 individual mice per group from 1 experiment. (**C** and **D**) Flow cytometric contour plots display IL-7R and GM-CSF levels of (**C**) MLN (day 15), cLP (days 15 and 28), and (**D**) cLP (day 27) donor-derived CD4$^+$ T cells after GVHD induction by C57Bl/6 WT (red) and *Batf*$^{-/-}$ (black) CD3$^+$ T cell transfer into (**C**) BALB/c and (**D**) BALB.b mice, respectively. Histograms show the IL-7R expression status of GM-CSF$^+$CD45.2$^+$CD4$^+$ T cells compared with IL-7R isotype control staining (gray-shaded area). Mean values ± SEM represent frequencies (top) and absolute numbers of IL-7R^{hi}GM-CSF$^+$ cells within CD45.2$^+$CD4$^+$ donor T cells found in the MLN (**C**) and cLP (**C**, days 15 and 28; **D**, day 27). Results for WT mice (**C**, MLN and cLP, day 15: n = 7; cLP, day 28: n = 7; **D**, n = 4) and *Batf*$^{-/-}$ mice (**C**, MLN and cLP, day 15: n = 7; cLP, day 28: n = 4; **D**, n = 5) from 1 of 2 experiments are shown. (**E**) Relative frequencies and absolute numbers of CD45.2$^+$CD3$^+$CD4$^+$IL-7R^{hi}CD44$^+$CD62L$^-$ cLP T cells (Tem cells) of the indicated genotypes 28 days after GVHD induction (C57Bl/6 into BALB/c), as described in **B**, were assessed by flow cytometry. Bar graphs indicate the mean ± SEM (n = 7 WT mice and n = 4 *Batf*$^{-/-}$ mice). *P < 0.05, **P < 0.01, ***P < 0.001, and ****P < 0.0001, by 1-way ANOVA with Bonferroni's multiple comparisons post test (**A** and **B**) and unpaired Student's t test (**C**–**E**).

with systemic antibody–mediated GM-CSF neutralization. Finally, reconstitution studies functionally demonstrated that intestinal GVHD–derived IL-7R^{hi} cLP T cells were able to reconstitute GVHD-associated colitis in *Batf*$^{-/-}$ donor T cell–treated mice.

Collectively, our study identifies and characterizes a distinct T cell subpopulation that, in GVHD biology, exerts a thus-far unappreciated mechanism of tissue damage via IL-7–driven, BATF-dependent formation of IL-7R^{hi}GM-CSF$^+$ T cells. Interestingly, IL-7 has been repeatedly implicated in promoting T cell recovery after allo-HCT, and its value is currently being tested in clinical studies (33–35). However, there is emerging evidence that IL-7 might cause more harm than benefit, given the positive association between elevated serum levels and acute GVHD development and relapse (32, 36–39). With the identification of IL-7R^{hi}GM-CSF$^+$ T cells as important drivers of GVHD, our study provides a mechanistic link between the IL-7–driven immune response and the occurrence of acute GVHD. GM-CSF has been shown to drive tissue inflammation in various immune-mediated disease models (40). Importantly, our results demonstrate that in GVHD, donor T cell–derived GM-CSF itself promotes systemic and intestinal GVHD, especially after pathogenic donor T cell differentiation, and hence GVHD manifestation, have taken place. Given our data, we propose a model in which host tissue–derived IL-7 (e.g., produced by intestinal epithelial cells [41, 42], hepatocytes [43], and hair follicle cells [44]) critically instructs donor T cells under the T cell–intrinsic control of BATF to become IL-7R^{hi} Tem cells that mediate intestinal GVHD at least in part by expressing GM-CSF. Hence, therapeutic targeting of the IL-7R/BATF/GM-CSF axis might represent a future option to mitigate acute, life-threatening intestinal GVHD.

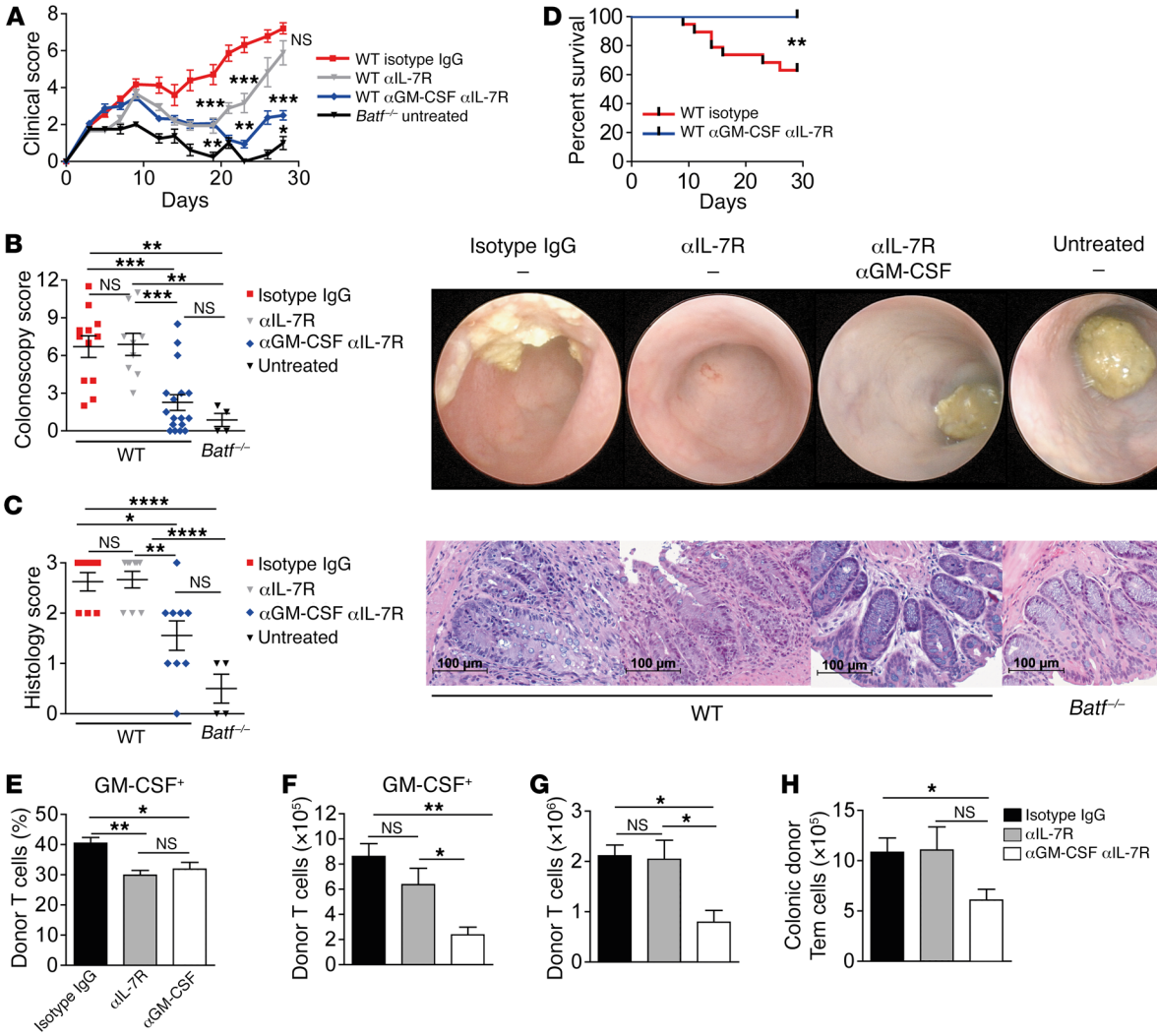

Figure 9. IL-7–responsive GM-CSF⁺ colonic T cells drive intestinal GVHD. (**A**–**D**) Antibody-mediated systemic blockade of IL-7R and GM-CSF affects clinical and intestinal GVHD manifestations in the complete MHC-mismatched model (C57Bl/6 into BALB/c). WT CD3⁺ T cell–recipient mice were given anti–IL-7R (αIL-7R) until day 15, either alone (gray line and triangles) or in combination with continuously administered anti–GM-CSF (αGM-CSF) (blue line and diamonds). As controls, WT donor T cells were continuously treated with isotype IgG antibody (red line and squares), or *Batf*$^{-/-}$ donor T cells were transplanted alone without further treatment (black line and triangles). The clinical GVHD score (**A**), the colonoscopy score and representative endoscopic images (**B**), the histology score and representative histopathologic images of GVHD-associated colitis on day 28 (**C**), and the survival rates (**D**) are shown. Scale bars: 100 μm. Data from 2 independent experiments were pooled and include (**A**, **B**, and **D**) WT isotype IgG (n = 19), WT anti–IL-7R (n = 9), WT anti–GM-CSF/anti–IL-7R (n = 17), and untreated *Batf*$^{-/-}$ (n = 4) mice; and (**C**) WT isotype IgG (n = 8), WT anti–IL-7R (n = 9), WT anti–GM-CSF/anti–IL-7R (n = 8), and untreated *Batf*$^{-/-}$ (n = 4) mice. Shown are the relative frequencies (**E**) and absolute numbers (**F**) of cLP CD45.2⁺CD3⁺CD4⁺GM-CSF⁺ T cells, the absolute numbers of donor-derived cLP T cells (**G**), and CD44⁺CD62L⁻ (Tem) T cells (**H**) in CD45.2⁺CD3⁺CD4⁺ cLP T cells 28 days after GVHD induction (C57Bl/6 into BALB/c), which were treated with isotype IgG antibody, anti–IL-7R antibody alone, or in combination with anti–GM-CSF antibody, as described in **A**. A representative experiment of 2 experiments is shown and involved WT isotype IgG (n = 7), WT anti–IL-7R (n = 8), and WT anti–GM-CSF/anti–IL-7R (n = 7) mice. Data in **A**–**E** represent the mean ± SEM. *P < 0.05, **P < 0.01, ***P < 0.001, and ****P < 0.0001, by 2-sided, unpaired Student's t test (**A**) and 1-way ANOVA with Bonferroni's multiple comparisons post test (**B**–**H**).

Methods

Human studies. Human colonic tissue biopsies (n = 52) were collected during colonoscopy of allo-HCT patients. Colonoscopies were performed at the Department of Hematology and Oncology and Gastroenterology of the University Hospital Regensburg.

Upon removal, tissue was either stored at –80°C or directly conveyed for RNA isolation using an RNeasy Mini Kit (QIAGEN), followed by cDNA synthesis using Moloney murine leukemia virus reverse transcriptase (Promega) according to the manufacturers' instructions. Quantitative PCR (qPCR) analyses were performed on a Mastercyler Ep Realplex (Eppendorf) using a QuantiFast SYBR Green PCR Kit (QIAGEN) according to the manufacturers' instructions and as previously described (45). The following gene-specific primer sets to detect human transcripts were used: *BATF*, forward, 5′-GACAAGAGAGCCCAGAGGTG-3′, reverse, 5′-TTCTGTGTCTGCCTCTGTCG-3′; 18S ribosomal RNA, forward, 5′-ACCGATTGGATGGTTTAGTGAG-3′, reverse, 5′-CCTACGGAAACCTTGTTACGAC-3′. Expression of *BATF* was normalized to 18S ribosomal RNA. The expression levels represent relative units and were calculated from a standard curve plotting 3 different concentrations of log dilutions against the PCR cycle number as previously described (45).

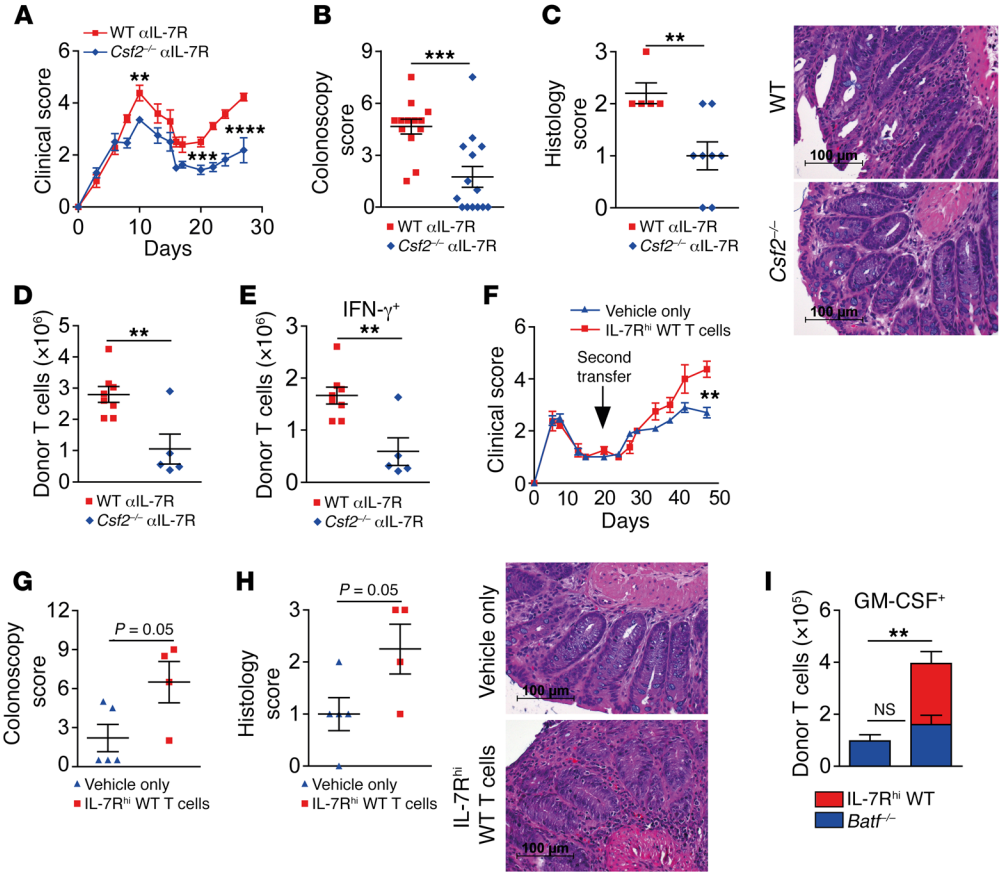

Figure 10. IL-7R^{hi}GM-CSF^{+} colonic T cells are sufficient to reestablish intestinal GVHD. (**A**–**E**) Effects of antibody-mediated IL-7R blockade on GVHD manifestations were dependent on T cell–intrinsic GM-CSF. C57Bl/6 WT (red squares) or *Csf2*$^{-/-}$ (blue diamonds) donor CD3^{+} T cells were transplanted into allo-BMT BALB/c mice and treated with anti–IL-7R 3 times per week until day 15. GVHD scores (**A**), colonoscopy scores on day 28 (**B**), histology scores, and representative colon cross-sections (**C**) of GVHD colitis are shown. (**D** and **E**) Total donor CD45.2^{+}CD3^{+}CD4^{+} T cells (**D**) and absolute numbers of IFN-γ^{+}CD45.2^{+}CD3^{+}CD4^{+} donor cLP T cells in the GVHD-prone mice described in **A** were assessed by intracellular flow cytometry. In **A** and **B**, pooled data are from 2 independent experiments (n = 13 WT + anti–IL-7R and n = 14 anti–IL-7R + *Csf2*$^{-/-}$ mice). In **C**, data are from 1 experiment (n = 5 WT + anti–IL-7R and n = 8 anti–IL-7R + *Csf2*$^{-/-}$ mice). In **D** and **E**, data are from 1 experiment (n = 8 WT + anti–IL-7R and n = 5 *Csf2*$^{-/-}$ + anti–IL-7R mice). (**F**–**I**) Allo-BMT (CD45.2^{+} *Rag1*$^{-/-}$ BM) BALB/c mice received allogeneic CD45.2^{+}CD3^{+}C57BL6 *Batf*$^{-/-}$ T cells. (**F**) Ten days later, as a second transfer, mice received i.v. either 2 × 10^{5} alloreactive B6.SJL CD45.1^{+}CD3^{+}IL-7R^{hi} cLP T cells (red squares; n = 6) that were sort purified from mice with established intestinal GVHD 28 days after GVHD induction or that were treated with PBS (vehicle) only (blue diamonds, n = 5). Clinical GVHD scores (**F**), colonoscopy scores (**G**), histology scores, and representative colon cross-sections (**H**) of GVHD colitis on day 47, i.e., 35 days after the second transfer. (**I**) Absolute numbers of CD45.1^{+}CD4^{+}GM-CSF^{+} WT (red) and CD45.2^{+}CD4^{+}GM-CSF^{+}*Batf*$^{-/-}$ (blue) cLP T cells. The left bar (blue only) depicts GM-CSF^{+}CD4^{+} T cells from vehicle-only–treated mice, while the right bar (blue and red) displays the absolute pool of GM-CSF^{+} cLP donor CD4^{+} T cells present in mice that received both CD45.1^{+}IL-7R^{hi} cLP WT (red) and *Batf*$^{-/-}$ donor T cells (blue). Scale bars: 100 μm. $^{**}P < 0.01$, $^{***}P < 0.001$, and $^{****}P < 0.0001$, by 2-sided, unpaired Student's t test. P values in **G** and **H** were also determined by 2-sided, unpaired Student's t test.

In parallel, colonic tissue sections were analyzed for the presence or absence of histopathologic signs of intestinal GVHD during the clinical examination by a clinical pathologist trained in GVHD-associated gastrointestinal histopathology. Histopathologic scoring of colitis activity and the presence of GVHD-associated apoptotic events was performed as previously published (46) and as described in detail in the histology section below.

Mice. Female BALB/cJRj, Ly5.2^{+} (CD45.2^{+}) C57Bl/6 mice were obtained from Elevage Janvier, and congenic Ly5.1^{+} (CD45.1^{+}) B6.SJL-*Ptprc*^{a} *Pepc*^{b}/BoyCrl mice were obtained from Charles River Laboratories. Mice were used at 7 to 12 weeks of age. *Batf*$^{-/-}$ mice (B6.129S-*Batf*$^{tm1.1Kmm}$/J) were described previously (6). *Csf2*$^{-/-}$ (GM-CSF) mice on a C57Bl/6 background were provided by G. Dranoff (Dana-Farber Cancer Institute, Boston, Massachusetts, USA) and Georg Weber (47, 48). Ubc-luc^{+} mice (LTPA Ubc-luc^{+}:Tyr C/C [C57BL/6]; PerkinElmer) were provided by Stefan Wirtz and intercrossed with *Batf*$^{-/-}$ mice.

Induction and monitoring of murine GVHD. Ten- to twelve-week-old female H-2d^{+} BALB/c (complete MHC–mismatched model) or H-2b^{+} BALB.b (miHA-mismatched model) mice were lethally irradiated with 8 Gy via total body irradiation (TBI). Twenty-four hours later, mice were i.v. injected with 5 × 10^{6} T cell–depleted BM cells from allogeneic CD45.1/Ly5.1^{+} B6.SJL-*Ptprc*^{a} *Pepc*^{b}/BoyCrl mice or with BM cells from allogeneic CD45.2 B6.129S7-Rag1tm1Mom/J *Rag1*$^{-/-}$ mice. T cell depletion of BM cells was achieved using anti-CD90.2 magnetic microbeads (Miltenyi Biotec) according to the manufacturer's instructions and routinely yielded T cell frequencies of less than 2% of the initial population. Forty-eight hours after irradiation, mice received i.v. injections of 0.7 × 10^{6} (complete MHC–mismatched model) or

5×10^6 (miHA-mismatched model) alloreactive $CD3^+$ T cells that were magnetically enriched from total mononuclear splenocyte preparations of C57Bl/6 WT, *Batf*$^{-/-}$, *Ubc-luc*$^+$, *Ubc-luc*$^+$ *Batf*$^{-/-}$, and *Csf2*$^{-/-}$ mice, respectively, using the Mouse Pan T Cell Isolation Kit II (Miltenyi Biotec) according to the manufacturer's instructions. In cotransfer studies, *Rag1*$^{-/-}$ BM was transplanted, followed by transfer of 0.35×10^6 congenically marked WT and 0.35×10^6 congenically marked *Batf*$^{-/-}$ T cells 24 hours later. Clinical GVHD scores were assessed every other day and included 6 parameters: body weight, posture, activity, skin and fur texture, and stool consistency. The severity of the individual parameters was scored on a range from 0 for no manifestation to 2 for severe manifestation. If an individual mouse reached a combined disease score above 8, the mouse was euthanized (49, 50).

In vivo bioluminescence imaging. In vivo bioluminescence imaging (BLI) was performed as previously described (51). In brief, 10 minutes after i.p. injection of 100 μl VivoGlo Luciferin (1.5 mg/ml; Promega) into mice that were GVHD prone as a result of adoptive transfer of allogeneic C57Bl/6 donor T cells transgenically expressing luciferase under the control of the ubiquitin promoter, bioluminescence over the abdominal region was recorded over a period of 5 minutes using an IVIS Lumina II charge-coupled imaging system (Caliper Life Science, PerkinElmer) every 3 to 4 days, beginning 4 days after irradiation. During the procedure, animals were anesthetized via inhalation of ambient air supplemented with 3% isoflurane. Images were further analyzed and processed using Living Image Software 2.5 (Caliper Life Science, PerkinElmer).

Mouse colonoscopy. Macroscopic assessment of the murine colon was performed using an Image 1 S3 Mini-Endoscope (Karl Storz) as previously described (52). The procedure was performed on mice that were anesthetized by inhalation of ambient air supplemented with 3% isoflurane. Colitis activity was determined by applying a modified murine endoscopic score of colitis severity (MEICS) assessing thickening of the bowel wall, changes in vascularity, granularity of the mucosal surface, and stool consistency, with each scored from 0 to 3, with a maximum total score of 12, as previously described (5).

Adoptive transfer with intravital confocal microscopy. Intravital confocal microscopy analyses upon adoptive transfer of T cells were performed according to a previously published study (53). Briefly, BALB/c mice were irradiated with 8 Gy and transplanted with 5×10^6 BM cells from *Rag1*$^{-/-}$ mice. Nine days later, mice were anesthetized via i.p. ketamine-xylazine administration. To counterstain preexisting cells, Hoechst dye was injected i.v. prior to T cell transfer. For counterstaining of the vasculature, dextran–Alexa Fluor 647 (dextran-AF647) (Thermo Fisher Scientific) was directly injected into the ileocolic artery together with the cells, as described below. To this end, alloreactive $CD4^+$ T cells were magnetically enriched from mononuclear splenocyte preparations of naive CD45.1 B6.SJL WT or CD45.2 *Batf*$^{-/-}$ mice using the mouse CD4 Isolation Kit (Miltenyi Biotec). WT T cells were labeled with CFSE, while Batf$^{-/-}$ T cells were labeled with CellTrace Yellow (CTY) using the CellTrace CFSE and CellTrace Yellow Cell Proliferation kits, respectively, according to the manufacturer's instructions (Thermo Fisher Scientific). After median laparotomy and direct cannulation of the ileocolic artery, 1×10^6 labeled T cells of each genotype were together adoptively transferred by intra-arterial injection. Colonic tissue homing of transferred T cells was assessed 1 hour later. For this, and after exteriorization of the colon, the colonic mucosal tissue was aligned onto a transparent glass Petri dish. Images were taken with a confocal microscope (Leica SP 8) using the laser lines 405 nm, 488 nm, 552 nm, and 633 nm to excite Hoechst, CFSE, CTY, and Alexa Fluor 647, respectively. At least 5 independent regions of interest (ROI) per mouse were used to enumerate differentially labeled T cells homed and migrated to the cLP compartment.

In vivo administration of agonistic proteins or blocking antibodies during murine GVHD. Recombinant GM-CSF reconstitution studies were performed by daily i.p. administration of 150 ng recombinant, carrier-free mouse GM-CSF protein (BioLegend) dissolved in a volume of 100 μl, starting on day 5 and maintained until day 28. Controls were treated with sterile PBS (vehicle) alone.

For IL-7R blockade experiments, i.p. injections (300 μg/injection) of anti–mouse IL-7R antibody (clone A7R34; BioXcell) were given 3 times per week, starting on the day of BMT (day 1) until day 15, either alone or in combination with systemic GM-CSF neutralization by additional administration (300 μg/injection) of an anti-mouse GM-CSF antibody (MP1-22E9; BioXcell) administered 3 times per week throughout the experiment in a total volume of 100 μl. Control-treated mice received an isotype control rat IgG2a antibody (clone 2A3; BioXcell; 300 μg/injection) or vehicle alone (PBS) 3 times per week over the entire course of the experiment.

Reconstitution studies by adoptive donor T cell transfer. For the reconstitution experiments, female BALB/c mice were lethally irradiated (day 0) and consecutively transplanted with 5×10^6 T cell–depleted BM cells from allogeneic CD45.2 B6.129S7-Rag1tm1Mom/J *Rag1*$^{-/-}$ mice (day 1). Twenty-four hours later, 0.7×10^6 alloreactive $CD45.2^+CD3^+$ *Batf*$^{-/-}$ T cells were given i.v. (day 2). Ten days later (day 12), *Batf*$^{-/-}$ T cell–recipient mice were rechallenged via i.v. transfer of 2×10^5 $CD45.1^+$ congenically marked, allogeneic $CD3^+IL\text{-}7R^{hi}$ T cells that were isolated from the cLP cell suspensions from mice with established acute intestinal GVHD induced by the transplantation of allogeneic $CD45.1^+$ donor T cells 28 days before, as described above. GVHD development in $IL\text{-}7R^{hi}$ LP T cell–recipient and PBS-recipient (vehicle only) mice was continuously monitored.

Histology. For the human studies, intestinal GVHD within colonic tissue samples from allo-HCT patients was graded histologically according to Lerner (54). Lerner grade 0 was categorized as "no GVHD" versus any observed grades of GVHD. Apoptosis was semiquantitatively scored by 2 expert pathologists. The number of apoptotic cells per high-power field (HPF) was counted, and 0–1 apoptotic cells per HPF were scored as grade 0, whereas 2–4, 5–7, and more than 7 apoptotic cells per HPF were scored as grades 1, 2, and 3, respectively, and were hence considered positive for apoptosis. By this approach, occasionally occurring apoptotic events were not misinterpreted to be caused by or related to intestinal GVHD.

For the murine studies, the whole colon was removed, intensively flushed, and rinsed ex vivo to remove feces as described below. Parts of the distal colon and the liver were fixed in 4.5% formaldehyde, dehydrated in alcohol, and embedded in paraffin. Sections were cut at a thickness of 3 μm. For pathological analysis, colon and liver sections were stained with H&E using a standard protocol. Cross-sections were evaluated on a Zeiss Axio Imager.A1 microscope. Histomorphological changes were assessed in a blinded manner by clinically trained pathologists experienced in murine histopathologic studies. The histology scores reflect the degree of colonic tissue inflammation assessed semiquantitatively within a well-oriented, representative area of each sample, as previously described (55): 0 (no or minimal

signs); 1 (mild signs); 2 (moderate signs); or 3 (severe signs). Microscopic visualization of hepatic GVHD manifestation was scored from 0 to 3 by assessing inflammation- and bile duct–associated lesions, respectively, as previously described (55).

Immunohistochemistry. Immunohistochemical analysis was performed on formalin-fixed and deparaffinized tissue sections from the distal mouse colon using the tyramide signal amplification (TSA) Cy3 System (PerkinElmer), as recommended by the manufacturer and as described previously (56). In brief, for antigen retrieval, sections were treated for 20 minutes with heated citrate buffer (10 mM, pH 6). Then, tissue sections were blocked with Protein Block, Serum-Free (product X090930-2; Dako). The primary antibody rabbit anti-MPO (ab9535; Abcam) was used at a 1:200 dilution in 2% BSA with TBST and incubated overnight at 4°C. The biotinylated secondary goat anti-rabbit antibody (58-065-144; Dianova) was used at a 1:1,000 dilution. Nuclei counterstaining was performed with Hoechst 33342 (Molecular Probes) in a 1:5,000 dilution. Images were recorded using the Leica DMI 4000 B fluorescence microscope.

For quantification of MPO^+ cells, representative colonic tissue areas were identified, and images under ×400 magnification representing a HPF were recorded. Collectively, images of 8 mice derived from at least 3 independent experiments per group were taken, followed by enumeration of the number of MPO^+ cells per HPF by an experienced scientist blinded to the origin and source of the scored images.

Isolation of cLP T cells. After mice were sacrificed, colon specimens were removed, flushed, and rinsed with PBS to remove feces, and then cut into small pieces and again washed using HBSS supplemented with 1% EDTA (0.5 mM). After this, colonic tissues were digested with DNase I (0.5 mg/ml), collagenase D (1 mg/ml) and dispase II (6 Units/ml) solution (all from Roche) containing 5% FCS. Next, digested colonic tissue was further subjected to a density centrifugation step with 80% and 40% Easycoll (Biochrom) in order to separate and isolate the LP cell fraction, followed by additional washing steps using cell culture media.

Flow cytometry and cell sorting. Mononuclear single-cell or T cell suspensions were stained with the following multicolor antibody panels for surface proteins and intracellular cytokines: anti-CD3ε (clone 145-2C11; eBioscience); anti-CD4 (clone GK1.5; BD Biosciences); anti-CD8 (clone 53-6.7; BD Biosciences); anti-CD19 (clone MB19-1; eBioscience); anti-CD25 (clone PC61.5; eBioscience); anti-CD45.1 (clone A20; BD Biosciences); anti-CD69 (clone H1.2F3; BD Biosciences); anti-CD3 (clone 17A2; BioLegend); anti-CD4 (GK 1.5; BioLegend); anti-CD8a (clone 53-6.7; BioLegend); anti-CD45.1 (clone A20; BioLegend); anti-CD45.2 (clone 104; BioLegend); anti-CD44 (clone IM7; BioLegend); anti-CD62L (clone MEL-14; BioLegend); anti-CD127 (clone A7R34; BioLegend); anti–GM-CSF (clone MP1-22E9; BioLegend); anti–IL-17A (clone TC11-18H10.1; BioLegend); anti–IFN-γ (clone XMG1.2; BioLegend); anti–TNF-α (clone MP6-XT22; BioLegend); anti–IL-6 (clone MP5-20F3; BioLegend); 7-AAD Viability Staining Solution (eBioscience); anti-$H2k^d$ (clone SF1-1.1; BioLegend); anti-α4β7 (clone DATK32; BioLegend); anti-CCR9 (clone CW-1.2; BioLegend); anti–Ki-67 (clone SolA15; eBioscience, Thermo Fisher Scientific); and anti-FoxP3 (clone FJK-16s; eBioscience). Both Ki-67 and FoxP3 were stained using a FoxP3 Staining Kit (eBioscience) according to the manufacturer's recommendations.

Cells were analyzed using BD FACSCanto II and FACSFortessa II flow cytometers (BD Biosciences). After exclusion of doublets, 7-aminoactinomycin D–negative cells or cells negative for LIVE/DEAD Fixable Aqua Dead Cell Stain (LIVE/DEAD Fixable Aqua Dead Cell Stain Kit; Life Technologies, Thermo Fisher Scientific) within the live gate were used for further downstream analyses. Acquired data were further analyzed using FlowJo 7.6.5 software.

In vitro T cell cultures. After Ack buffer lysis–mediated red blood cell removal, splenocytes were magnetically enriched for $CD4^+$ T cells by negative selection following the manufacturer's instructions ($CD4^+$ T Cell Isolation Kit II; Miltenyi Biotec). Afterward, $CD4^+$ T cells were stained with anti-CD4 and anti-CD25 antibodies, and $CD4^+CD25^-$ naive T cells were sort purified using a BD FACSAria II cell sorter located at the Cell Sorting and Immunomonitoring Core Unit of the University Hospital Erlangen, Friedrich-Alexander University Erlangen-Nuremberg. The purity of sorted $CD4^+CD25^-$ T cells was regularly greater than 98%. Naive $CD4^+$ T cells (10^6 cells/ml) were cultured in supplemented RPMI 1640 medium (10% FCS, 1% penicillin-streptomycin, 1% nonessential amino acids, 1% L-glutamine, and 0.1% β-mercaptoethanol) and activated with 10 μg/ml plate-bound anti-CD3 (clone 145-2C11; BioXcell) and 1 μg/ml soluble anti-CD28 (clone 37.51; BioXcell) antibodies. T cell cultures were additionally supplemented with 10 μg/ml soluble anti–IFN-γ (clone XMG1.2; BioXcell) antibody, either alone or together with 2 ng/ml recombinant IL-7 (rIL-7) (R&D Systems). On days 3 and 5, respectively, 10^6 T cells/ml were replated in the presence of complete RPMI 1640 medium supplemented with either anti–IFN-γ (10 μg/ml) antibody alone or in combination with rIL-7 (2 ng/ml).

Intracellular cytokine staining. Isolated cLP cells and in vitro–differentiated $CD4^+$ T cells, respectively, were extensively washed, and then 10^6 cells/ml were cultured in supplemented DMEM medium (containing 10% FCS, 1% penicillin-streptomycin, 1% nonessential amino acids, 1% L-glutamine, and 0.1 % β-mercaptoethanol) in the presence or absence of 50 ng/ml PMA and 1 μM ionomycin for 4 hours. Brefeldin A (1 μg/ml) was added for the last 3 hours of culturing (all purchased from Sigma Aldrich). After staining of extracellular proteins with fluorochrome-labeled antibodies, intracellular cytokine staining was performed as previously described (6). In brief, cells were fixed through incubation with a fixation buffer containing 2% paraformaldehyde (PFA) for 15 minutes at room temperature. After additional washing steps to remove excess PFA, cells were permeabilized by sequential washing steps in FACS buffer containing 0.05 % saponin (Sigma Aldrich), followed by intracellular cytokine staining (30 min) with fluorochrome-labeled anti-cytokine antibodies dissolved in FACS buffer containing 0.5 % saponin.

Serum cytokine analysis. Blood was collected by cheek puncture after BMT. Sera were generated by whole-blood centrifugation, followed by quantification of IL-6, IL-17A, IFN-γ, and TNF-α sera levels using a cytometric bead array (CBA) with a BD Enhanced Sensitivity CBA Mouse Flex Set system, a CBA Mouse Flex Set system, and a BD Mouse Th1/Th2/Th17 Cytokine Kit (BD Biosciences), respectively, according to the manufacturer's instructions. Samples were run on FACSCanto II and FACS Fortessa II flow cytometers. Data were analyzed using FCAP Array, version 3.0.1 software (BD Biosciences).

Isolation of RNA and cDNA synthesis. Total RNA was isolated from flow cytometry–sorted donor cLP–resident $CD4^+$ T cells using an RNeasy Micro Kit (QIAGEN) or from whole colon tissue using the NucleoSpin RNA Isolation Kit (Macherey Nagel). cDNA was generated using the iScript cDNA Synthesis Kit (Bio-Rad) according to the manufacturer's instructions. For qPCR analysis, iQ SYBR Green Supermix (Bio-Rad) was used according to the manufacturer's instructions.

Primers to perform quantitative expression analyses of murine transcripts via qPCR were synthesized by Eurofins Genomics. The following primer sequences were used: *Hprt*, forward, 5′-TGGATACAGGCCAGACTTTGTT-3′, reverse, 5′-CAGATTCAACTTGCGCTCATC-3′; *Batf*, forward, 5′-GGAAGATTAGAACCATGCCTC-3′, reverse, 5′-CCAGGTGAAGGGTGTCGG-3′; *Ifng*, forward, 5′-ATCTGGAGGAACTGGCAAAA-3′, reverse, 5′-TGAGCTCATTGAATGCTTGG-3′; *Csf2*, forward, 5′-ATCAAAGAAGCCCTGAACCT-3′, reverse, 5′-GTGTTTCACAGTCCGTTTCC-3′; *Tnfa*, forward, 5′-CTTGTGGCAGGGGCCACCAC-3′, reverse, 5′-CCATGCCGTTGGCCGGAGG-3′; *Il6*, forward, 5′-CCGGAGAGGAGACTTCACAG-3′, reverse, 5′-TTCTGCAAGTGCATCATCGT-3′; and *Il17a*, forward, 5′-GCTCCAGAAGGCCCTCAGA-3′, reverse, 5′-AGCTTTCCCTCCGCATTGA-3′. In addition, a primer pair for *Il7r* (QT00103922) was obtained from QIAGEN.

Statistics. Statistical analyses were performed using GraphPad Prism 5 (GraphPad Software). Statistical significance was determined by an unpaired, 2-sided Student's *t* test, a 1-way ANOVA followed by Bonferroni's multiple comparisons post test, or a 1-way ANOVA Kruskal-Wallis test followed by Dunn's multiple comparisons post test. Differences in survival rates between 2 groups were assessed by log-rank test. The sample size and number of mice used per experiment were dependent on availability and chosen in compliance with the committees approving the experiments. We did not perform randomization of samples or mice. Except for the histopathologic scoring data generated by a pathologist, the scientists performing the experiments were not blinded to the study design. No specific exclusion criteria were applied in this study. In most instances, data represent the mean ± SEM. A *P* value of less than 0.05 was considered statistically significant.

Study approval. Human studies were conducted after written informed consent was provided by the donor patients. All human studies were performed according to Declaration of Helsinki principles and approved by the ethics committee of the University Hospital Regensburg. All animal experiments were approved by the government of Mittelfranken in Bavaria, Germany.

Author contributions

BA, JR, and CH performed experiments with the help of TV and VB and analyzed and interpreted data. EH, MK, and SG provided human colonic tissue samples, performed analyses related to human colon biopsies, and helped with the interpretation and critical discussion of the results. SRJ, SW, GFW, SV, and AB provided critical reagents and mice and helped with the interpretation of the results. MBH and TL performed histopathologic analyses. SZ performed intravital confocal microscopy studies with the help of TV. MFN and AM provided critical advice and helped with the interpretation and critical discussion of the results. KH and EU designed the study, performed analyses, and interpreted results. KH directed the study and wrote the manuscript, with contributions from all authors.

Acknowledgments

We thank A. Abendroth, F. Ganss, J. Früh, and I. Klaußner and the Cell Sorting and Immunomonitoring Core Unit at the University Hospital Erlangen for excellent experimental and technical assistance. We thank C. Becker (University Hospital Erlangen, Medical Department 1) for providing critical reagents and G. Dranoff for providing GM-CSF$^{-/-}$ mice. This study was supported by the Wilhelm Sander-Stiftung (2010.105.1, to KH and EU); the Max-Eder Research Program of the German Cancer Aid (to KH and EU); the ELAN program of the University Erlangen-Nuremberg (project 09.08.19.1, to KH); the Adolf Messer Foundation (to EU); the Interdisciplinary Center for Clinical Research Erlangen (project A53, to KH); CELLEUROPE (FP7-People-2012-ITN, no. 315963, to SG); the LOEWE Center for Cell and Gene Therapy, Frankfurt, Germany, funded by the Hessian Ministry of Higher Education, Research and the Arts (III L4-518/17.004, to EU and JR); the Collaborative Research Center 1181 (DFG-CRC 1181, project B05) at the University Hospital Erlangen, Friedrich-Alexander University Erlangen-Nuremberg (to KH); and the Collaborative Research Center 221 (CRC/TR221-DFG, project B03, to KH).

Address correspondence to: Kai Hildner, Department of Medicine 1, University Hospital Erlangen, Ulmenweg 18, D-91054 Erlangen, Germany. Phone: 49.9131.85.35.000; Email: Kai.Hildner@uk-erlangen.de.

1. Ferrara JL, Levine JE, Reddy P, Holler E. Graft-versus-host disease. *Lancet*. 2009;373(9674):1550–1561.
2. Markey KA, MacDonald KP, Hill GR. The biology of graft-versus-host disease: experimental systems instructing clinical practice. *Blood*. 2014;124(3):354–362.
3. Coghill JM, Sarantopoulos S, Moran TP, Murphy WJ, Blazar BR, Serody JS. Effector CD4+ T cells, the cytokines they generate, and GVHD: something old and something new. *Blood*. 2011;117(12):3268–3276.
4. Castilla-Llorente C, et al. Prognostic factors and outcomes of severe gastrointestinal GVHD after allogeneic hematopoietic cell transplantation. *Bone Marrow Transplant*. 2014;49(7):966–971.
5. Punkenburg E, et al. Batf-dependent Th17 cells critically regulate IL-23 driven colitis-associated colon cancer. *Gut*. 2016;65(7):1139–1150.
6. Schraml BU, et al. The AP-1 transcription factor Batf controls T(H)17 differentiation. *Nature*. 2009;460(7253):405–409.
7. Leppkes M, et al. RORgamma-expressing Th17 cells induce murine chronic intestinal inflammation via redundant effects of IL-17A and IL-17F. *Gastroenterology*. 2009;136(1):257–267.
8. Ivanov II, et al. The orphan nuclear receptor RORgammat directs the differentiation program of proinflammatory IL-17+ T helper cells. *Cell*. 2006;126(6):1121–1133.
9. Wang C, et al. BATF is required for normal expression of gut-homing receptors by T helper cells in response to retinoic acid. *J Exp Med*. 2013;210(3):475–489.
10. Withers DR, et al. Transient inhibition of ROR-γt therapeutically limits intestinal inflammation by reducing TH17 cells and preserving group 3 innate lymphoid cells. *Nat Med*. 2016;22(3):319–323.
11. Fulton LM, et al. Attenuation of acute graft-versus-host disease in the absence of the transcription factor RORγt. *J Immunol*. 2012;189(4):1765–1772.
12. Iclozan C, et al. T helper17 cells are sufficient but not necessary to induce acute graft-versus-host disease. *Biol Blood Marrow Transplant*. 2010;16(2):170–178.
13. Kappel LW, et al. IL-17 contributes to CD4-mediated graft-versus-host disease. *Blood*. 2009;113(4):945–952.
14. Yu Y, et al. Prevention of GVHD while sparing GVL effect by targeting Th1 and Th17 transcription factor T-bet and RORγt in mice. *Blood*. 2011;118(18):5011–5020.
15. Yi T, et al. Absence of donor Th17 leads to augmented Th1 differentiation and exacerbated acute graft-versus-host disease. *Blood*. 2008;112(5):2101–2110.
16. Bäuerlein CA, et al. A diagnostic window for the treatment of acute graft-versus-host disease prior to visible clinical symptoms in a murine model.

BMC Med. 2013;11:134.
17. Anderson BE, et al. Memory CD4+ T cells do not induce graft-versus-host disease. *J Clin Invest*. 2003;112(1):101–108.
18. Edinger M, et al. CD4+CD25+ regulatory T cells preserve graft-versus-tumor activity while inhibiting graft-versus-host disease after bone marrow transplantation. *Nat Med*. 2003;9(9):1144–1150.
19. Beilhack A, et al. Prevention of acute graft-versus-host disease by blocking T-cell entry to secondary lymphoid organs. *Blood*. 2008;111(5):2919–2928.
20. Sheng W, et al. STAT5 programs a distinct subset of GM-CSF-producing T helper cells that is essential for autoimmune neuroinflammation. *Cell Res*. 2014;24(12):1387–1402.
21. Seddon B, Tomlinson P, Zamoyska R. Interleukin 7 and T cell receptor signals regulate homeostasis of CD4 memory cells. *Nat Immunol*. 2003;4(7):680–686.
22. Kondrack RM, Harbertson J, Tan JT, McBreen ME, Surh CD, Bradley LM. Interleukin 7 regulates the survival and generation of memory CD4 cells. *J Exp Med*. 2003;198(12):1797–1806.
23. Li J, Huston G, Swain SL. IL-7 promotes the transition of CD4 effectors to persistent memory cells. *J Exp Med*. 2003;198(12):1807–1815.
24. Zhang Y, Joe G, Hexner E, Zhu J, Emerson SG. Alloreactive memory T cells are responsible for the persistence of graft-versus-host disease. *J Immunol*. 2005;174(5):3051–3058.
25. Park H, et al. A distinct lineage of CD4 T cells regulates tissue inflammation by producing interleukin 17. *Nat Immunol*. 2005;6(11):1133–1141.
26. Gaffen SL, Jain R, Garg AV, Cua DJ. The IL-23-IL-17 immune axis: from mechanisms to therapeutic testing. *Nat Rev Immunol*. 2014;14(9):585–600.
27. Codarri L, et al. RORγt drives production of the cytokine GM-CSF in helper T cells, which is essential for the effector phase of autoimmune neuroinflammation. *Nat Immunol*. 2011;12(6):560–567.
28. El-Behi M, et al. The encephalitogenicity of T(H)17 cells is dependent on IL-1- and IL-23-induced production of the cytokine GM-CSF. *Nat Immunol*. 2011;12(6):568–575.
29. Sonderegger I, Iezzi G, Maier R, Schmitz N, Kurrer M, Kopf M. GM-CSF mediates autoimmunity by enhancing IL-6-dependent Th17 cell development and survival. *J Exp Med*. 2008;205(10):2281–2294.
30. Haines CJ, et al. Autoimmune memory T helper 17 cell function and expansion are dependent on interleukin-23. *Cell Rep*. 2013;3(5):1378–1388.
31. Noster R, et al. IL-17 and GM-CSF expression are antagonistically regulated by human T helper cells. *Sci Transl Med*. 2014;6(241):241ra80.
32. Chung B, Dudl EP, Min D, Barsky L, Smiley N, Weinberg KI. Prevention of graft-versus-host disease by anti IL-7Ralpha antibody. *Blood*. 2007;110(8):2803–2810.
33. Alpdogan O, et al. Administration of interleukin-7 after allogeneic bone marrow transplantation improves immune reconstitution without aggravating graft-versus-host disease. *Blood*. 2001;98(7):2256–2265.
34. Alpdogan O, et al. IL-7 enhances peripheral T cell reconstitution after allogeneic hematopoietic stem cell transplantation. *J Clin Invest*. 2003;112(7):1095–1107.
35. Perales MA, et al. Recombinant human interleukin-7 (CYT107) promotes T-cell recovery after allogeneic stem cell transplantation. *Blood*. 2012;120(24):4882–4891.
36. Thiant S, et al. Plasma levels of IL-7 and IL-15 in the first month after myeloablative BMT are predictive biomarkers of both acute GVHD and relapse. *Bone Marrow Transplant*. 2010;45(10):1546–1552.
37. Dean RM, et al. Association of serum interleukin-7 levels with the development of acute graft-versus-host disease. *J Clin Oncol*. 2008;26(35):5735–5741.
38. Sinha ML, Fry TJ, Fowler DH, Miller G, Mackall CL. Interleukin 7 worsens graft-versus-host disease. *Blood*. 2002;100(7):2642–2649.
39. Thiant S, et al. Plasma levels of IL-7 and IL-15 after reduced intensity conditioned allo-SCT and relationship to acute GVHD. *Bone Marrow Transplant*. 2011;46(10):1374–1381.
40. Wicks IP, Roberts AW. Targeting GM-CSF in inflammatory diseases. *Nat Rev Rheumatol*. 2016;12(1):37–48.
41. Madrigal-Estebas L, et al. Human small intestinal epithelial cells secrete interleukin-7 and differentially express two different interleukin-7 mRNA Transcripts: implications for extrathymic T-cell differentiation. *Hum Immunol*. 1997;58(2):83–90.
42. Watanabe M, et al. Interleukin 7 is produced by human intestinal epithelial cells and regulates the proliferation of intestinal mucosal lymphocytes. *J Clin Invest*. 1995;95(6):2945–2953.
43. Sawa Y, et al. Hepatic interleukin-7 expression regulates T cell responses. *Immunity*. 2009;30(3):447–457.
44. Adachi T, et al. Hair follicle-derived IL-7 and IL-15 mediate skin-resident memory T cell homeostasis and lymphoma. *Nat Med*. 2015;21(11):1272–1279.
45. Landfried K, et al. Tryptophan catabolism is associated with acute GVHD after human allogeneic stem cell transplantation and indicates activation of indoleamine 2,3-dioxygenase. *Blood*. 2011;118(26):6971–6974.
46. Landfried K, et al. Recipient NOD2/CARD15 status affects cellular infiltrates in human intestinal graft-versus-host disease. *Clin Exp Immunol*. 2010;159(1):87–92.
47. Dranoff G, et al. Involvement of granulocyte-macrophage colony-stimulating factor in pulmonary homeostasis. *Science*. 1994;264(5159):713–716.
48. Weber GF, et al. Interleukin-3 amplifies acute inflammation and is a potential therapeutic target in sepsis. *Science*. 2015;347(6227):1260–1265.
49. Cooke KR, et al. An experimental model of idiopathic pneumonia syndrome after bone marrow transplantation: I. The roles of minor H antigens and endotoxin. *Blood*. 1996;88(8):3230–3239.
50. Meinhardt K, et al. Identification and characterization of the specific murine NK cell subset supporting graft-versus-leukemia- and reducing graft-versus-host-effects. *Oncoimmunology*. 2015;4(1):e981483.
51. Waldner MJ, et al. VEGF receptor signaling links inflammation and tumorigenesis in colitis-associated cancer. *J Exp Med*. 2010;207(13):2855–2868.
52. Becker C, Fantini MC, Neurath MF. High resolution colonoscopy in live mice. *Nat Protoc*. 2006;1(6):2900–2904.
53. Fischer A, et al. Differential effects of α4β7 and GPR15 on homing of effector and regulatory T cells from patients with UC to the inflamed gut in vivo. *Gut*. 2016;65(10):1642–1664.
54. Lerner KG, Kao GF, Storb R, Buckner CD, Clift RA, Thomas ED. Histopathology of graft-vs.-host reaction (GvHR) in human recipients of marrow from HL-A-matched sibling donors. *Transplant Proc*. 1974;6(4):367–371.
55. Kaplan DH, Anderson BE, McNiff JM, Jain D, Shlomchik MJ, Shlomchik WD. Target antigens determine graft-versus-host disease phenotype. *J Immunol*. 2004;173(9):5467–5475.
56. Günther C, et al. Caspase-8 controls the gut response to microbial challenges by Tnf-α-dependent and independent pathways. *Gut*. 2015;64(4):601–610.